

# Quantum-Accelerated Self-Consistent Field: A Hybrid Algorithm

Alexis Ralli,<sup>1,2</sup> Tim Weaving,<sup>1,2</sup> Thomas M. Bickley,<sup>2</sup> Peter V. Coveney,<sup>1,2,3</sup> and Peter J. Love<sup>1,4,5,6,7</sup>

<sup>1</sup>*QMatter, Inc., 254 Chapman Rd, Office 109, Suite 101-B, Newark, Delaware, 19702, USA*

<sup>2</sup>*Centre for Computational Science, Department of Chemistry, University College London, WC1H 0AJ, United Kingdom*

<sup>3</sup>*Advanced Research Computing Centre, University College London, WC1H 0AJ, United Kingdom*

<sup>4</sup>*Department of Physics and Astronomy, Tufts University, Medford, MA 02155, USA*

<sup>5</sup>*Computational Science Initiative, Brookhaven National Laboratory, Upton, NY 11973, USA*

<sup>6</sup>*Department of Computer Science, University of Toronto, 40 St. George Street, Toronto, ON M5S 3H6, Canada*

<sup>7</sup>*Department of Physics, University of Toronto, Toronto, Ontario M5S 1A7, Canada*

(Dated: June 19, 2026)

We present the Grover adaptive search self-consistent field (GAS-SCF) algorithm. GAS-SCF leverages quantum arithmetic to construct an efficient oracle that marks target states (Fock states) which improve upon some initial classical energy estimate. Amplitude amplification then increases the probability of measuring these states. This approach offers a theoretical quadratic speed-up for the optimization problem encountered in SCF quantum chemistry and establishes a baseline against which structured optimization algorithms, such as QAOA and DQI may be compared. In this work, we classically simulate three examples as proofs of concept of the algorithm, the largest consisting of 26 qubits. We then extend our analysis to two larger systems, with  $O_3$  representing the largest case at 330 qubits. These examples are chosen to probe classically challenging SCF regimes. Achieving chemically relevant applications of GAS-SCF will require large-scale, fault-tolerant quantum hardware.

## I. INTRODUCTION

Quantum chemistry is a widely studied application of quantum computing [1–4]. Much effort has been devoted to studying the Full Configuration Interaction (FCI) problem on quantum computers [1, 2]. In this case one is seeking exponential quantum speedups for problems out of reach of current or foreseeable classical computers due to the rapid increase in Hilbert space dimension of FCI with basis set size. However, making quantum algorithms for FCI realizable on reasonable sized quantum computers requires careful optimization and exploitation of problem structure [5–12]. This problem structure may be exploited by classical algorithms as well, leading to closer competition between classical and quantum approaches [13, 14]. Furthermore, the importance of large-scale FCI calculations to chemistry is largely unknown, precisely because such calculations are classically intractable at present. Recently, these considerations have motivated the development of quantum algorithms that offer speedups over classical heuristics directly [4, 15]. Such an approach is complementary to efforts to directly solve the FCI problem by quantum computation.

The self-consistent field (SCF) method is perhaps the oldest heuristic in quantum chemistry [16]. SCF methods, including Hartree–Fock (HF) and Kohn–Sham density functional theory (KS-DFT), provide approximate solutions to the time-independent Schrödinger equation and are routinely used to define the “canonical” molecular orbital basis in second-quantized formulations of the molecular Hamiltonian [17, 18]. The difference between the HF energy and the FCI energy is the *correlation en-*

*ergy*. Recovery of the correlation energy is the goal of all post-Hartree-Fock methods. Post-Hartree-Fock methods are often defined in the basis of molecular orbitals obtained from HF. Alternative molecular orbital (MO) bases, including localized and natural orbitals, are also commonly used. Improvements in the solutions to HF SCF problems can yield improved molecular orbitals, impacting all Post-Hartree-Fock methods.

As shown in [19], the Hartree-Fock method is NP-complete, and hence in the worst case one does not expect any classical or quantum polynomial time algorithm to provide a solution. This rather negative view is contradicted by the widespread success of HF in chemical problems, a fact which is partly explained by considering the approximability of the NP complete problem HF represents. In [20] we showed that HF problems can be mapped to signed MaxCut problems, which admit performance guarantees in terms of the approximation ratio - the ratio of the approximate solution (the obtained HF energy from a particular SCF algorithm) to the true HF energy. Despite impressive classical advances - such as the HF calculation of 9,188 water molecules reported by Barca *et al.* (involving 119,444 basis functions) [21], the optimality of such large-scale solutions remains unclear.

The work presented in [20] is related to the variational optimization of two-electron reduced density (2-RDM) matrices [22–24]; however, in our formulation [20], both the 2-RDM and 1-RDM admit a significantly simpler structure, as they are derived from single Fock references. The specific optimization problem in our single reference SCF algorithm is composed of two steps: a continuous optimization over orbital parameters, and a discrete optimization to find the lowest energy Fock state

for the new parameters. In order for the minimum state to change the eigenvalues (which are simply the diagonal entries in the second quantized molecular Hamiltonian) must cross. For sufficiently small changes in the orbital parameters, one can imagine that the states can be followed perturbatively from the initial orbitals without difficulty in identifying the updated state. Conversely, this suggests that tracking the ground state as the orbital parameters evolve is only reliable when those changes remain very small. However, the NP-completeness of the problem implies that such incremental variations are insufficient to guarantee finding the true minimum in the worst case [19].

While quantum computers are not believed to be capable of solving NP complete problems exactly in polynomial time, there are many heuristic quantum approaches to combinatorial optimization problems [25–27]. There is recent evidence that they may be able to obtain improvements in the approximation ratio obtained for some problems [27, 28]. Optimization of SCF approaches provides an interesting target for such algorithms, as the optimization problem itself arises in quantum mechanics and one may speculate optimistically that this will make it more amenable to quantum approaches. More specifically, classical performance guarantees on the approximation ratio for MaxCut with signed weights are weaker than in the unsigned case, making performance improvements easier to achieve. In the present paper we seek to exploit prior classical knowledge of approximate solutions and rigorous quantum speedups for unstructured problems to define a benchmark quantum algorithm, GAS-SCF, for improving SCF calculations.

Grover’s search algorithm [29] and its generalization, amplitude amplification [30], are fundamental components underlying many quantum algorithms. Their use often provides quadratic speedups for many quantum algorithms over the best-known classical approaches. However, this advantage is asymptotic and constant prefactors can strongly influence practical performance. Prior work suggests that a modest fault-tolerant quantum computer is unlikely to realize a meaningful runtime benefit for quadratic speedups, as error-correction overheads can outweigh the gains for reasonable instance sizes [31, 32]; similar conclusions are drawn elsewhere [33, 34]. Improvements in error correction can of course change these estimates [35]. Grover speedups also remain an important goal for quantum algorithms: one would always wish to be able to obtain *at least* a Grover speedup. A Grover speedup sets a baseline against which more sophisticated quantum optimization techniques, such as the adiabatic algorithm [25], the quantum approximate optimization algorithm (QAOA) [26], or decoded quantum interferometry (DQI) [27] may be compared.

In this work, we present the implementation details of the recently proposed Grover Adaptive Search Self-Consistent Field (GAS-SCF) algorithm, which was previously described briefly by us in [20]. Here we define and analyze the algorithm in detail and provide an open

source implementation [36] for the GAS [37, 38] subroutine to support other research into the algorithm. Theoretically, it has been proven that GAS provides a quadratic speedup over classical methods [37], requiring  $\mathcal{O}(\sqrt{N})$  operations compared to the classical  $\mathcal{O}(N)$ , where  $N$  denotes the size of the search space. This quadratic speedup relies on an oracle. We show how to construct this oracle given a classical bound on the energy, which is always available for HF problems from variational classical approaches. Specifically, we construct an oracle that labels all Fock states that improve upon a classical reference energy. GAS-SCF is therefore a warm-started version of Grover search, in which all problem structure is assumed to have been fully utilized to obtain the classical bound, and therefore quantum unstructured search is used on the states that lie above this bound. If another quantum optimization algorithm outperforms GAS-SCF it must do so by exploiting further problem structure not available to classical heuristics, and not used by GAS-SCF.

The remainder of the paper is organized as follows. Section II introduces the GAS-SCF algorithm and outlines its compilation into quantum circuits. Section III presents numerical examples, focusing in particular on  $\text{H}_3^-$ , LiH,  $\text{OH}^-$ ,  $\text{O}_2$  and  $\text{O}_3$  molecular systems. Section IV examines the potential of quantum advantage for the algorithm. Finally, the computational methodology for the numerical studies is given in Section V.

## II. THE GAS-SCF ALGORITHM

In this section we introduce the GAS-SCF algorithm, first defining the SCF problem to be solved in section II A, then giving the GAS algorithm in section II B, section II C then includes how to deal with SCF integrals by approximating them with integer values.

### A. The SCF Problem

The Quadratic Unconstrained Binary Optimization (QUBO) problem seeks the minimum of a function  $f(\vec{x})$  of the following form:

$$f(\vec{x}) = \vec{x}^T Q \vec{x} + \vec{b}^T \vec{x} + c = \sum_{i,j} Q_{ij} x_i x_j + \sum_i b_i x_i + c. \quad (1)$$

Where  $x_i \in \{0, 1\}$  for  $i = 1, \dots, n$  and  $f(\vec{x}) \in \mathbb{R}$ , so that  $f(\vec{x})$  is a pseudo-boolean function. The matrix  $Q \in \mathbb{R}^{n \times n}$  encodes the quadratic coefficients,  $\vec{b} \in \mathbb{R}^n$  represents the linear terms, and  $c \in \mathbb{R}$  is a constant offset. Since  $x_i^2 = x_i$ , linear terms can be absorbed into the diagonal entries of  $Q$ , allowing the QUBO formulation to be written using only the  $Q$  matrix.

The QUBO problem arising from Hartree-Fock SCF

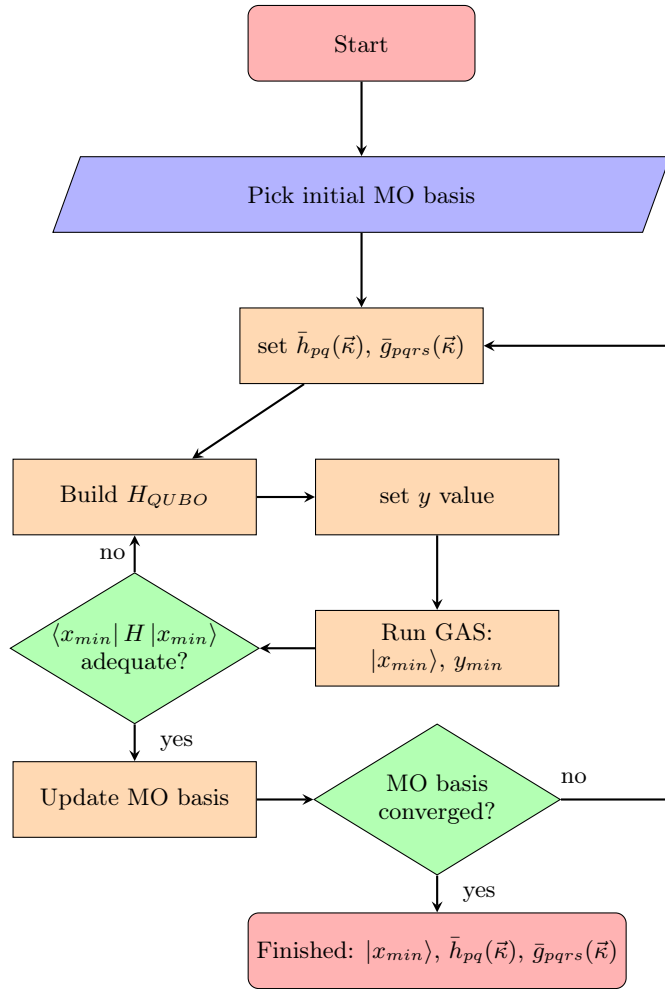


FIG. 1: Full outline of GAS-SCF algorithm (equation 3). Refer to Algorithms 1 and 2 in [20] for the procedure to update the MO basis. The initial MO basis may be set to any standard choice, such as Löwdin or canonical or similar. Here, “adequate” refers to an energy that has converged, outperforms classical SCF solutions, or satisfies a predefined (possibly spectral-based) threshold for advancing the algorithm to the MO basis optimization stage.

was given in [20]:

$$\begin{aligned}
 H_{QUBO}(\vec{k}) = & \sum_w^M \bar{h}_{ww}(\vec{k}) x_w + \\
 & \frac{1}{2} \sum_{\substack{m,w \\ m \neq w}}^M \left( [\bar{g}_{mmww}(\vec{k}) - \bar{g}_{mwwm}(\vec{k})] x_m x_w \right).
 \end{aligned} \tag{2}$$

This problem is defined in the occupation number basis, so that the boolean variables represent fermionic occupancies of molecular orbitals. The coefficients  $h_{pq}$  and  $g_{pqrs}$  are one- and two-electron integrals, expressed in an orthonormal molecular orbital (MO) basis. Different choices of MO basis may be related via  $H \mapsto H(\vec{k}) = U^\dagger(\vec{k}) H U(\vec{k})$ , so the choice of MO basis is parametrized by  $\vec{k}$  [20].

The SCF problem can be written as [20]:

$$E_{SCF} = \min_{\vec{k}} \left[ \min_{|x\rangle \in \mathcal{V} \subset \mathcal{D}} [\langle x | H_{QUBO}(\vec{k}) | x \rangle] \right]. \tag{3}$$

Here,  $\mathcal{D}$  denotes the set of all computational basis states or  $n$ -bit bitstrings. The size of this set is  $2^n$ , while  $\mathcal{V}$  represents a subset consisting of computational states that lie within the correct symmetry sector. For example states with the desired number of alpha/beta electrons, total spin angular momentum squared  $S^2$ , and molecular point group symmetries. These symmetries reduce the search space - e.g. particle number symmetry reduces the scaling from  $2^n$  to  $\binom{n/2}{n_\alpha} \cdot \binom{n/2}{n_\beta}$  for  $n$  spin MOs and  $(n_\alpha, n_\beta)$  electrons. The dimension of  $\vec{k}$  is bounded by  $|\vec{k}| \leq \frac{n(n-1)}{2}$ , reflecting the invariance of the SCF wavefunction under certain orbital rotations. For example, in HF closed-shell systems, only rotations between occupied and virtual orbitals contribute. This means that classical heuristics can both exploit the continuous/discrete

nature of the problem and do not have to brute force search over all  $2^n$  bitstrings nor redundant orbital rotations.

To summarize the SCF problem defined in Equation 3, first the inner optimization aims to find the best single bitstring that minimizes  $H_{QUBO}(\vec{\kappa})$  for a fixed  $\vec{\kappa}$  (the current MO basis). The outer optimization then updates the MO basis ( $\vec{\kappa}$ ) with reference to the state obtained in the inner optimization. This is repeated until the energy converges. In this work, we give a quantum algorithm for the inner, discrete optimization, while the outer, continuous, optimization is handled by a classical routine. For the remainder of this paper, we focus on the discrete optimization step, as the classical routine has already been discussed in [20] where two approaches are given. Figure 1 illustrates a high-level overview of the complete algorithm.

Classical solvers for the SCF optimization problem employ heuristic strategies rather than performing an exhaustive search of the solution space. The most widely used approach iteratively diagonalizes the Fock matrix until self-consistency is achieved, while the second most common class of methods uses second-order optimization techniques based on orbital rotations to directly minimize the SCF energy. In both cases, the reference determinant is held fixed. However, particularly in the latter approach, Thouless' theorem implies that any other single-determinant state can be generated from a given reference determinant through an orbital rotation, yielding a (non-orthogonal) Fock state [39, eq 2]. Consequently, this parameterization provides access to the complete single-determinant optimization space. This means that the optimal solution to the SCF problem can always be found by omitting the discrete optimization step in equation 3. The discrete optimization step finds the minimum state of SCF Hamiltonians along the continuous optimization path, which in general are distinct from the rotation of the initial minimum. Subsequent rotations proceed from this new starting point. The optimization of equation 3 can therefore be regarded as restarting the continuous optimization periodically, after discrete minimization of the intermediate SCF problem. Although the theoretical optimum is the same for both GAS-SCF and traditional approaches, the use of different classical SCF heuristics complicates direct comparisons of runtime, convergence behavior, and solution quality. Nevertheless, our earlier work demonstrated improved convergence behavior [20], a result further supported by numerical findings in this work for  $O_2$  and  $O_3$ , which indicate that improved solutions can be obtained relative to classical heuristics.

In the next subsection, we describe how  $H_{QUBO}(\vec{\kappa})$  can be solved using GAS.

## B. Grover Adaptive Search

Gilliam, Woerner, and Gonciulea [40] demonstrated how Grover Adaptive Search (GAS) [37, 38, 41] can be

applied to binary optimization problems. We build on their framework by incorporating additional constraints arising from spin and particle number symmetries, and restrict the search to solutions of particular Hamming weights. Figure 2 illustrates the quantum circuit used in the Grover Adaptive Search routine of GAS-SCF, which we summarize below.

The first register contains the  $n$  qubits on which the QUBO problem is defined. Each term in the QUBO can be represented using a single- or doubly-controlled phase gate, with the control qubits determined by the structure of each QUBO term. These gates are applied to a secondary register of  $(m + 1)$  qubits, which encodes the value of the QUBO cost function in the Fourier basis [42]. This operation is represented by the  $f(\vec{x})$  gate in this work. Higher-order polynomial terms, such as cubic or quartic interactions, can be represented by increasing the number of control qubits, but that is not relevant for the QUBO setting of the present work.

The minimum number of qubits  $m$  required to store the maximum value of the QUBO cost function is given by:

$$m = \lceil \log_2(\max[f(\vec{x})]) \rceil \leq \left\lceil \log_2 \left( \sum_{ij} |Q_{ij}| + \sum_i |b_i| \right) \right\rceil. \quad (4)$$

A single additional qubit is included to allow the representation of negative values, enabling the encoding of integers in the range  $[-2^m, 2^m]$ . The  $(m + 1)$ -qubit register stores the cost function in the Fourier basis, which is then transformed into the computational basis using the inverse Quantum Fourier Transform ( $QFT^\dagger$ ) [40, 42]. The single qubit below the  $m$  register stores the sign of the cost function. We give details of the necessary components in the supporting information S.I and S.II.

To adapt this algorithm for chemical problems, constraints on the number of alpha (spin-up) and beta (spin-down) electrons must be enforced. These constraints reflect number and spin symmetry, thereby reducing the optimization space. To incorporate these constraints, a similar procedure is used as for encoding the QUBO cost function onto an ancilla register. However, since the number operator has only non-negative expectation values, the additional qubit required for negative values is unnecessary. The number of qubits needed is:

$$\mu = \nu = \lceil \log_2 \left( \frac{n}{2} \right) \rceil. \quad (5)$$

Here,  $n \in 2\mathbb{Z}^+$  is the total number of spin-orbitals (or qubits), which is an even positive integer for chemical problems. Thus,  $n/2 \in \mathbb{Z}^+$  corresponds to the number of spatial orbitals.

The number of alpha ( $n_\alpha$ ) and beta ( $n_\beta$ ) electrons are also stored in ancillary registers using the Fourier basis, and subsequently transformed into the computational basis via the inverse Quantum Fourier Transform ( $QFT^\dagger$ ). Alternative quantum adder circuits could also be used

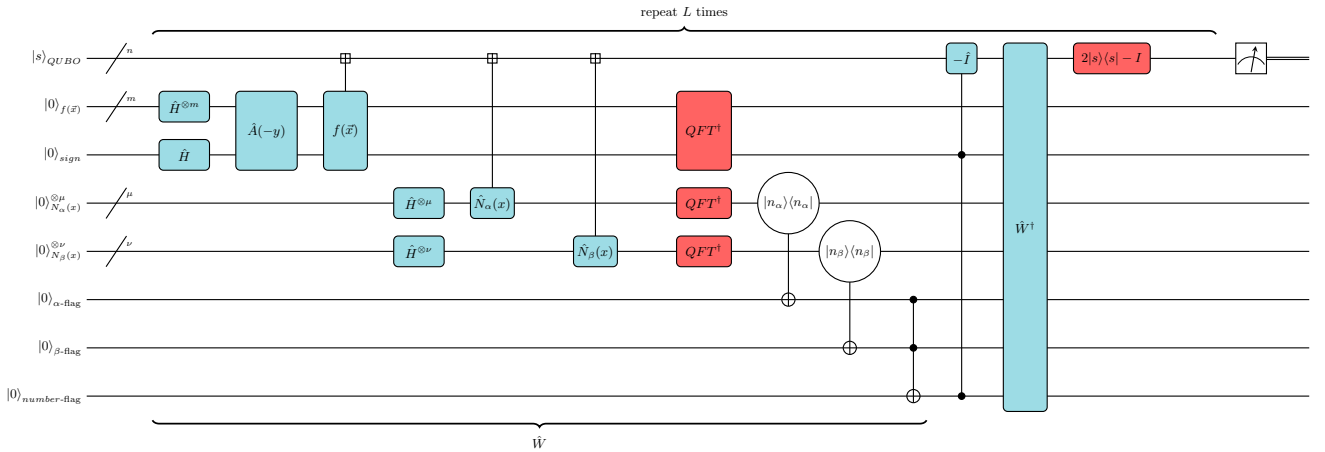


FIG. 2: Outline of the full quantum circuit to implement the Grover Adaptive Search Self-Consistent Field (GAS-SCF) algorithm. Here the search space is over the uniform superposition of computational states:  $|s\rangle = H^{\otimes n} |0\rangle^{\otimes n}$ . Figure 3 provides an alternate construction, where the state on the first  $n$ -qubit register is different. The  $\hat{A}$  and  $f(\vec{x})$  gates are defined in Figure S.1 and Figure S.5 in the supporting information. The former encodes the negative reference value  $(-y)$  setting a threshold, while the latter encodes the cost function for different binary states in the QUBO register state, as observed by the controls. The gates defined with clear circular controls, with projectors inside the controls, represent multi-controlled  $X$  gates whose control settings correspond to the target occupation numbers expressed in binary, see Figure S.6 for further detail. An alternative compilation is provided in the Supplemental Information S.V, which gives the corresponding  $T$ -gate cost. In this realization no  $QFT^\dagger$  is required.

here; however, given their variety [43], a detailed discussion is beyond the scope of this work.

The next step of the algorithm is to mark states that both:

1. Have a negative value in the QUBO cost function.
2. Satisfy the correct number of alpha and beta electrons.

To achieve this, a multi-controlled  $X$  gate is used, with controls defined by the bitstring representation of the desired binary occupation state. In Figure 2 this is represented by the projectors in each control. See Figure S.6 in the supporting information for further details. This gate acts on a single ancillary qubit, effectively flagging valid configurations. In the language of second quantization, these correspond to Fock states (occupation number states) in the correct particle-number symmetry sector. A Toffoli gate is then applied to store a  $|1\rangle$  state which acts as a flag if and only if both the alpha and beta electron count registers match their target values.

To mark the resulting states, a multi-controlled  $-I$  gate is applied. This gate is controlled by:

- The number-flag qubit (indicating the correct electron counts)
- The *sign* qubit from the  $(m+1)$  register (indicating a negative QUBO value).

We note that the *sign* qubit serves as a flag indicating whether the  $(m+1)$ -qubit register encodes a negative

value of the (QUBO) cost function. Specifically, this single qubit emerges from the Two's-complement representation of integers, in which the most significant (leftmost) bit determines the sign of the encoded value. For readers unfamiliar with Two's-complement arithmetic, additional background is provided in the supporting information S.II.

Overall, the controlled  $-I$  operation, implemented via a controlled  $R_z(-2\pi)$ , selectively applies a phase flip to all bitstrings  $\vec{x}$  with value  $f(\vec{x}) - y < 0$  and with the correct number of alpha and beta electrons. Here  $y$  is a constant shift representing the best value found so far (a random bitstring with the correct symmetries can be used to initialize this value or the output of a classical SCF calculation). Undoing the circuit which generated the marked states followed by a reflection around  $|s\rangle$  (the input state for Grover) then amplifies all marked states.

In summary, a high-level rundown of the GAS (inner optimization of Equation 3) is as follows:

1. Initialize a uniform superposition over all (or a selected subset of) bitstrings in the  $n$ -qubit QUBO register; in this work, this state is denoted by  $|s\rangle$  or  $|d\rangle$ .
2. Initialize the register of  $(m+1)$ -qubits, which stores the current value of the QUBO function, with the chosen starting value:  $-y$  (in the Fourier basis).
3. Conditioned on the  $n$ -qubit QUBO register, which encodes the bitstring inputs for the QUBO cost

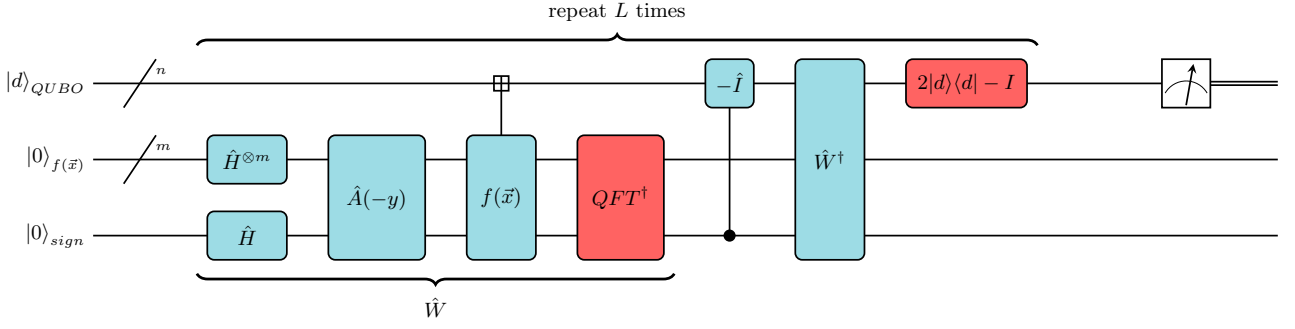


FIG. 3: Outline of the full quantum circuit to implement Grover Adaptive Search Self-Consistent Field (GAS-SCF) algorithm searching over Dicke states. Here, a Dicke state  $|d\rangle$  is prepared on the  $n$ -qubit register. This restricts the search space to bitstrings with the correct number of alpha and beta electrons and therefore the symmetry flagging step in Figure 2 is no longer needed. The  $\hat{A}$  and  $f(\vec{x})$  gates are defined in Figure S.1 and Figure S.5 in the supporting information. An alternative compilation is provided in the Supplemental Information S.V, which gives the corresponding  $T$ -gate cost. In this realization no  $QFT^\dagger$  is required.

	Gate	Count	Asymptotic	Note
(1)	$H$	$2(m+1)$	$\mathcal{O}(m)$	Preparation for storing QUBO value in Fourier basis
	$P^a$	$2(m+1)$	$\mathcal{O}(m)$	$\hat{A}(-y)$
	Singly-controlled $P$	At most $2(n[m+1])$	$\mathcal{O}(nm)$	$f(\vec{x})$ linear terms
	Doubly-controlled $P$	At most $2\binom{n}{2}[m+1]$	$\mathcal{O}(n^2m)$	$f(\vec{x})$ quadratic terms
	$m$ -qubit $QFT^\dagger$	2	$\mathcal{O}(1)$	To convert QUBO value to decimal basis
	$(n-1)$ -controlled $Z$	1	$\mathcal{O}(1)$	For $2 0^{\otimes n}\langle 0^{\otimes n}  - I^{\otimes n}$ reflection
	$X$	$2n$	$\mathcal{O}(n)$	For $2 0^{\otimes n}\langle 0^{\otimes n}  - I^{\otimes n}$ reflection
	$CNOT$	$2(n-1)$	$\mathcal{O}(n)$	For marking operation
(2)	$H$	$2(\mu+\nu)$	$\mathcal{O}(\log n)$	Preparation for storing occupation value in Fourier basis
	Singly-controlled $P$	$2n$	$\mathcal{O}(n)$	$\hat{N}_{\alpha/\beta}(x)$ linear terms
	$\mu$ -controlled $X$	2	$\mathcal{O}(1)$	To mark correct Hamming weight states ( $\alpha$ electrons)
	$\mu$ -qubit $QFT^\dagger$	2	$\mathcal{O}(1)$	To convert occupation values to decimal basis
	$\nu$ -controlled $X$	2	$\mathcal{O}(1)$	To mark correct Hamming weight states ( $\beta$ electrons)
	$\nu$ -qubit $QFT^\dagger$	2	$\mathcal{O}(1)$	To convert Fourier occupation values to decimal basis
	Toffoli	2	$\mathcal{O}(1)$	Check for correct number of $\alpha$ & $\beta$ electrons
(3)	$H$	$2n$	$\mathcal{O}(n)$	To reflect around $ s\rangle$ on $n$ -qubits
	Doubly-controlled $R_Z(-2\pi)$	1	$\mathcal{O}(1)$	For marking operation
(4)	Dicke state construction. See e.g. [44, 45]	$2(w(n/2, n_\alpha) + w(n/2, n_\beta))^b$	$\mathcal{O}(kn) \leq \mathcal{O}(n^2)^c$	To reflect around $ d\rangle$ on $n$ -qubits
	Singly-controlled $R_Z(-2\pi)$	1	$\mathcal{O}(1)$	For marking operation

<sup>a</sup> Phase gate.

<sup>b</sup>  $w(n, k)$  used as a placeholder for quantum circuit cost to generate  $\binom{n}{k}$  Dicke state.

<sup>c</sup> Scaling for the Dicke circuit implementation we used is at worst quadratic when  $k = \mathcal{O}(n)$  [44]; other approaches may differ.

TABLE I: Gate requirements for one repetition of GAS-SCF (Figure 2 / Figure 3) that is repeated  $L$  times. The table is broken into four sections as follows: (1), gates required for both  $|s\rangle$  and  $|d\rangle$  algorithms; (2), extra gates required to enforce occupation numbers (for  $|s\rangle$  version only); (3), extra gates required for reflection (for  $|s\rangle$  version only); (4), extra gates required for reflection (for  $|d\rangle$  version only). Here  $\alpha$  and  $\beta$  denote the number of spin-up and spin-down electrons respectively. An alternative compilation is provided in the Supplemental Information S.V, which gives the corresponding  $T$ -gate cost for both realizations. In this approach no  $QFT^\dagger$  is required.

function, compute and store the cost function value in the  $(m+1)$ -qubit register using quantum arithmetic.

- Mark all bitstrings (in the QUBO register) with a negative sign if their value is less than  $y$  and if they have the correct number of electrons.
- Undo steps 2 and 3 ( $W^\dagger$  in circuit).
- In the  $n$ -qubit QUBO register, apply a reflection around the input state ( $|s\rangle$  or  $|d\rangle$ ) to increase the

amplitude of marked states.

- Repeat the amplification routine (steps 2-6)  $L$  times to increase the probability of measuring marked bitstrings.
- Measure the QUBO register. With high probability, this yields a marked bitstring, representing an improved QUBO solution.
- Set  $y$  to be the new QUBO value of this improved bitstring and repeat from step 1 until convergence.

The amplification routine should be repeated  $L$  times where [46, 47]:

$$L = \frac{\pi}{4} \left[ \frac{1}{\arcsin \left( \sqrt{\frac{T}{N}} \right)} \right] - \frac{1}{2} \quad (6)$$

$$< \frac{\pi}{4} \sqrt{\frac{N}{T}} - \frac{1}{2},$$

$L$  should be rounded to the nearest integer based on the top line of this equation (we assume  $0 < T < \frac{N}{2}$ ). Here,  $T$  is the number of marked states and  $N \leq 2^n$  is the size of the search space. However, as noted in [40], the number of marked states,  $T$ , is generally unknown, and thus they define a randomized strategy to select  $L$ . An alternate approach has also been presented in [48] that has been shown to require fewer queries. On this issue, we appreciate Brassard’s reference to Kristen Fuchs, who likens Grover’s search algorithm to cooking a soufflé: if you use too many (overcooked) or too few (undercooked) queries, the outcome won’t yield good results [49]. Alternatively, fixed-point methods [50] ensure that at each step (increasing  $L$ ), the probability of measuring a marked state monotonically increases. However, this guarantee comes at the cost of losing the quadratic speedup. Yoder *et al.* later introduced an approach that achieves fixed-point behavior without sacrificing quantum speedup [51].

For electronic structure SCF applications, the total number of states with the correct number of spin up and down electrons ( $n_\alpha, n_\beta$ ) is given by:

$$\binom{n_{spatial}}{n_\alpha} \cdot \binom{n_{spatial}}{n_\beta} = \binom{n/2}{n_\alpha} \cdot \binom{n/2}{n_\beta} \geq T \quad (7)$$

which bounds the number of marked states,  $T$ , and thus the maximum value  $L$  can take for GAS-SCF. Weyl’s formula can also be utilized to give a better bound [52, eq 8] [53, eq 92], but requires a specified spin sector. Note in practice  $T$  will be smaller than this, as the marked states must also have a negative value in the  $(m + 1)$  register. If a good classical reference (corresponding to an appropriate  $y$ -value) is used, it can significantly reduce the number of relevant states and, consequently, the number of repetitions required.

This structure can be extended to construct an alternative quantum circuit for GAS-SCF. Instead of preparing an equal superposition over all computational basis states, we generate an equal superposition over states with the correct number of electrons. This corresponds to a Dicke state  $|d\rangle$ , which is an equal superposition of computational basis states of a fixed Hamming weight. The overall circuit is illustrated in Figure 3. While this algorithm introduces additional depth, due to Dicke state preparation and the Grover reflection step, it eliminates the need for ancilla qubits used to track electron count. In essence, the search space is inherently restricted to valid states within the correct number symmetry sector.

This structure is exactly what classical simulation techniques also take advantage of to simplify the optimization problem. Table I summarizes the circuit costs for both circuit implementations.

### C. Non-Integers

A challenge with the GAS routine is that it requires the QUBO formulation (Equation 2) to have integer coefficients, whereas in the SCF problem the coefficients (integrals) are real (floating point) numbers. Gilliam *et al.* explored two encoding strategies: integer-approximation and direct (Fejér) encoding schemes for treating non-integer functions [40]. In [54, Section III.C], Norimoto and Ishikawa discuss the Fejér encoding scheme in more detail.

In this work, we employ the integer-approximation scheme to enable the implementation of GAS-SCF. We note that multiplying the Hamiltonian’s coefficients by a constant  $\Lambda$  preserves the eigenspectrum, only rescaling the eigenvalues. Operationally for GAS-SCF this merely changes the number of qubits required in the  $(m + 1)$ -qubit register by  $\log \Lambda$ . If we multiply by a factor of  $2^\epsilon$  ( $\epsilon > 0, \epsilon \in \mathbb{R}$ ) we find Equation 4 is modified as:

$$m_\epsilon = \lceil \log_2 (2^\epsilon \max[f(\vec{x})]) \rceil = \epsilon + \lceil \log_2 (\max[f(\vec{x})]) \rceil$$

$$\leq \epsilon + \left\lceil \log_2 \left( \sum_{ij} |Q_{ij}| + \sum_i |b_i| \right) \right\rceil. \quad (8)$$

For  $\epsilon = 50$ , we have  $2^{50} \approx 1 \times 10^{15}$ . This increases the number of ancilla qubits by fifty but scales all coefficients by roughly  $1 \times 10^{15}$ . Given that most chemistry libraries only calculate the Hamiltonian coefficients (integrals) to fifteen decimal places [55], this  $\epsilon$  will round all the coefficients to integers as required. In the fault-tolerant regime, this additional qubit overhead is negligible. However, the number of non-Clifford rotations is increased, which may incur additional costs. If this becomes a limitation, alternative approaches to quantum arithmetic may help mitigate it [43] [56, Appendix D]. Moreover, for most practical applications, rounding to fewer decimal places is sufficient, as demonstrated by the numerical results presented in this work. Nonetheless, in the Supplemental information S.V we compile the GAS circuit using adder circuits derived in [56] and provide the overall T-gate cost. This alternative approach removes the need for  $QFT^\dagger$ .

In Section III, we present three numerical examples. The first two illustrate the inner workings of the algorithm and demonstrate the feasibility of rounding the Hamiltonian to integer coefficients. The third, and largest, example highlights the advantages of the algorithm, albeit for a classically tractable problem.

### III. NUMERICAL STUDY

#### A. GAS simulation

To study the performance of the GAS routine in GAS-SCF, we investigate a single inner optimization step within Equation 2 for the MO optimization of  $\text{H}_3^-$  and LiH in the STO-3G basis set. The goal is to find the bitstring with the lowest energy in the correct symmetry sector. Neither of these systems exhibits classical convergence issues and are small test examples, not as systems with potential practical advantage. Applying Eq 7 we find for  $\text{H}_3^-$  there are  $\binom{3}{2} \cdot \binom{3}{2} = 9$  and for LiH there are  $\binom{6}{2} \cdot \binom{6}{2} = 225$  valid bitstrings.

The ground states of  $\text{H}_3^-$  and LiH in the STO-3G basis have energy  $-24$  Ha and  $-888$  Ha respectively (in the integer coefficient problem). We first consider setting the threshold for GAS sufficiently low that the algorithm marks only the ground state. In this case GAS reduces to Grover search for the ground state in the symmetry subspace. To accomplish this, the GAS routine was configured with thresholds of  $y = -20$  and  $y = -880$  for  $\text{H}_3^-$  and LiH respectively. We initialized the system in the uniform state  $|s\rangle$  and the Dicke state  $|d\rangle$  for  $\text{H}_3^-$  and only in the Dicke state for LiH. We simulated quantum circuits with increasing number of repetitions  $L$ . We plot the probability of the marked state as a function of  $L$  in Figure 4. In each case, as  $L$  increases, the probability of measuring the optimal bitstring is observed to vary periodically as expected in Grover’s search. The optimal number of iterations can be determined by rounding Equation 6 to the closest integer. For  $\text{H}_3^-$  in the STO-3G basis with the uniform initialization  $|s\rangle$  and  $y = -20$  we have  $N = 2^6$  and  $T = 1$  and the optimal number of repetitions is  $L \approx 5.77 \mapsto 6$ . For  $\text{H}_3^-$  in the STO-3G basis with the Dicke state initialization  $|d\rangle$  and  $y = -20$  we have  $N = 9$ ,  $T = 1$  and  $L \approx 1.81 \mapsto 2$ .

If the classical estimate  $y$  used in GAS is so poor that more than half the states are in the search space are marked, GAS fails due to a well understood failure mode for Grover’s search when more than half the states are marked - called *overbalancing*. For  $\text{H}_3^-$  in the STO-3G basis with the Dicke state  $|d\rangle$  initialization, we found that setting  $y = -4$  as the initial starting point would cause the GAS-SCF routine to fail. In this case, the amplitude of the  $y = -4$  eigenstate increased, rather than the eigenstates with lower eigenvalues. As the problem is small (nine valid eigenstates) the allowed eigenvalues are:  $\{-24, -20, -16, -20, -12, -8, -16, -8, -4\}$ . The algorithm would therefore mark all the states below  $y = -4$ , meaning that there are more marked states than unmarked ones, thus causing the unmarked (incorrect) states to be amplified instead.

We propose the use of GAS-SCF as a method to improve upon the best available classical SCF solution, using the best classical reference to identify the states to mark. Avoiding overbalancing in GAS requires that the density of states of the molecule is such that the classi-

cal reference has lower energy than more than half of the states in the search space. Large numbers of configurations can have very similar energies if the ground state has large static correlation. If this causes overbalancing, Faro and Marino’s method of searching in overbalanced domains, applicable when valid solutions exceed half of the input space, can be used [57].

Overbalancing can never happen for the uniform superposition input  $|s\rangle$  state. This is because states belonging to incorrect symmetry sectors remain within the search space but are not marked, due to the constraints imposed by the number-symmetry registers. In particular, for  $n_s$  spatial orbitals the search space has dimension  $2^{2n_s}$ , whereas the maximum possible number of marked states is  $\binom{n_s}{n_\alpha} \cdot \binom{n_s}{n_\beta}$ . The worst-case subspace dimension occurs when:  $\binom{n_s}{n_s/2}^2$ . The corresponding fraction of the total search space can be written as:  $\tau = \binom{n_s}{n_s/2}^2 / 2^{2n_s}$  which we can bound as:  $\tau < \frac{2}{\pi n_s}$ . For  $n_s > 1$ , this implies  $\tau < 0.5$ , so the marked subspace always occupies less than half of the full search space. For the  $n_s = 1$  case, the solution is trivial.

Next, we focus on the more complex  $\text{OH}^-$  SCF optimization problem, which we previously showed had convergence issues [20]. Running RHF in PySCF returned a value of  $-75.0730$  Ha ( $y = -780$  for the rounded problem), which is a local minimum. This result could be improved by running more expensive second-order and stability methods in PySCF [20]. However, in the context of this work we use this result as a seed to show that GAS-SCF can improve a classical solution that has not converged properly; Figure 5 summarizes the results. In the chosen active space, there are  $\binom{6}{3} \cdot \binom{6}{3} = 400$  valid bitstring, a twelve qubit problem.

Figure 5a shows the overlap squared of the statevector from our GAS-SCF circuit, for different repetitions  $L$ , with the equal superposition of the 12 eigenstates with lower eigenvalues relative to the PySCF SCF solution. This demonstrates the probability of measuring a state that surpasses the PySCF solution. Using Equation 6,  $N = 400$  and  $T = 12$ , we see that  $L \approx 4.01 \mapsto 4$ . As expected, we observe that at  $L = 4$ , the probability of measuring a marked state is maximized. We performed a sampling statevector simulation for this scenario, which is summarized in Figure 5b. We observe that, across the 10,000 samples taken, all the bitstrings obtained result in a lower energy Fock state than the PySCF solution. In this case, the largest improvement over the PySCF solution is  $\approx 2.2$  eV. This illustrates how GAS-SCF can be used to search for solutions that are better than the best classical reference available.

Finally, we note that in this work we did not implement a strategy for selecting the number of Grover iterations  $L$ . Instead, our goal was to highlight the key components of the algorithm and evaluate its performance in specific scenarios, without the need for case-by-case adjustment of  $L$ , which could obscure the key properties of the algorithm. The choice of  $L$  has already been investigated in

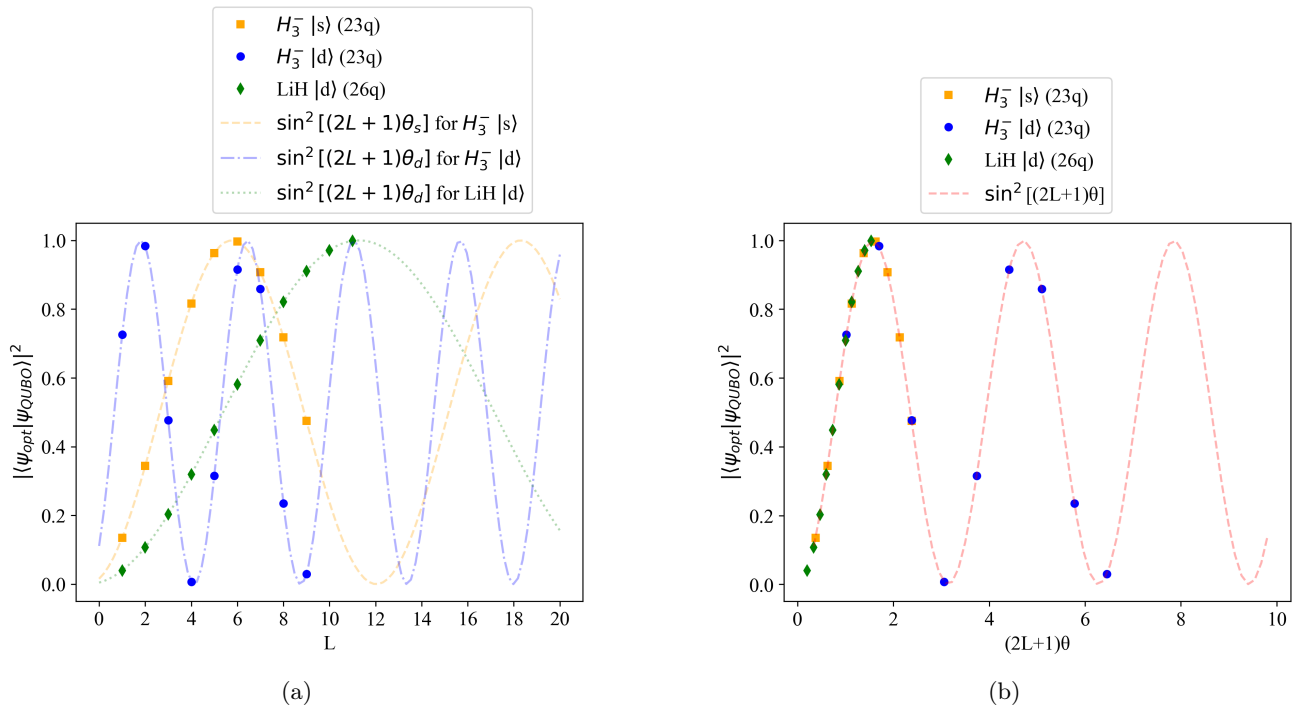


FIG. 4: GAS-SCF results for increasing number of iterations  $L$  (left) and  $(2L+1)\theta$  (right) where initial  $y$  was selected so that GAS-SCF would only amplify the ground state. The overlap between the true ground state  $|\psi_{opt}\rangle$  and the circuit statevector  $|\psi_{QUBO}\rangle$  is plotted for  $H_3^-$   $\blacksquare$  (uniform input  $|s\rangle$ ),  $H_3^-$   $\bullet$  (Dicke input  $|d\rangle$ ) and LiH  $\blacklozenge$  (Dicke input  $|d\rangle$ ). Qubit counts in the legend parenthesis provide the total number of qubits including all ancilla registers. Note  $\theta$  for each system is  $\arcsin(1/\sqrt{2^6})$ ,  $\arcsin(1/\sqrt{9})$  and  $\arcsin(1/\sqrt{225})$  respectively (equation 6).

prior work [40, 48, 50, 51]; therefore, further analysis is outside the scope of this study.

### B. Examples of SCF Convergence Issues

A further motivating example for GAS-SCF is triplet  $O_2$  at a bond length of 2.55 Å. This system was previously reported in [61] to exhibit low overlap between the restricted open-shell Hartree-Fock (ROHF) reference and the full configuration interaction (FCI) ground state in the STO-3G basis. We reproduce this result and find  $\langle FCI | ROHF \rangle = 2.17 \times 10^{-7}$  - see the raw data in [36] for further details. We extend this study to the larger 6-31G basis set and again find qualitatively similar behavior. However, a FCI calculation was not computationally feasible in this larger basis. Instead, we performed truncated configuration interaction calculations including up to single and double excitations ( $CI-12$ ) and up to single, double, triple, and quadruple excitations ( $CI-1234$ ). The ROHF overlap with these approximate wavefunctions is  $\langle CI-12 | ROHF \rangle = 0.959$  and  $\langle CI-1234 | ROHF \rangle = 0.0475$ . Interestingly, while the  $|CI-12\rangle$  state retains a large overlap with the ROHF reference, the more accurate  $|CI-1234\rangle$  state shows a dramatically reduced overlap. This highlights the importance of incorporating higher-order excitations: restrict-

ing attention to singles and doubles can artificially inflate the apparent significance of the reference determinant due to it being connected to all single and double excited determinants - as per the Slater-Condon rules [62, 63].

The underlying reason for this effect is nuanced, and thus we remark on further details here. In a CISD calculation, all determinants in the CISD space are, by construction, connected (have non-zero Hamiltonian matrix elements) to the reference (usually Hartree-Fock) state. Consequently, within this truncated subspace, the reference determinant is privileged and thus can appear disproportionately important. In contrast, any lower-energy determinant that may appear in the CISD wavefunction (relative to the reference Fock state) is guaranteed to not be connected to all other determinants within that CISD subspace; indeed, such a determinant is typically connected to only a small subset of the configurations present. This asymmetry explains why CISD can artificially inflate the apparent amplitude, and therefore the perceived significance, of the reference determinant. The  $O_2$  example illustrates this point and highlights the need for caution when interpreting results obtained within such restricted subspaces.

In both basis sets we observe that there exist other single Fock states with substantially higher overlap with the exact (or approximate) ground state than the ROHF ref-

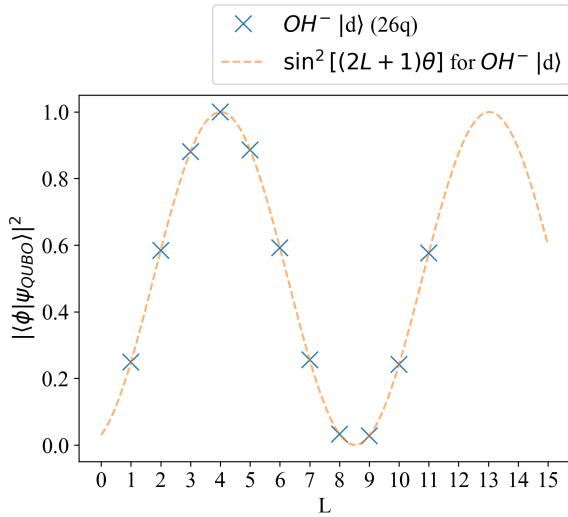
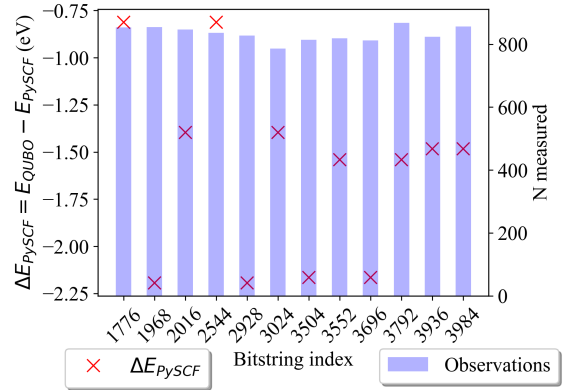
(a)  $\text{OH}^-$  (search space  $|d|$ , total qubits 26)(b) Results for  $L = 4$  repeats, showing the statevector sampled 10,000 times.

FIG. 5: GAS-SCF Dicke simulation result for  $\text{OH}^-$ . The  $y = -780$  (classical PySCF value) was used to seed the GAS-SCF routine. (a) Illustrates the overlap of the QUBO statevector with  $|\phi\rangle$  that is an equal superposition of the 12 Fock states with lower energy than the PySCF solution. (b) Results of the  $L = 4$  statevector sampling simulation with 10,000 shots. The  $x$ -axis gives the index of the sampled bitstring in base-10 (converting to binary gives the Fock state). The left  $y$ -axis gives the error between the GAS-SCF and PySCF RHF solution (scatter), where a negative value indicates GAS-SCF finding a better result. We see that in all cases a better bitstring over PySCF is obtained. The right  $y$ -axis gives the number of times each bitstring was sampled (bar-chart). Here  $\theta = \arcsin(\sqrt{12/400})$  (equation 6).

erence itself - for example:  $\langle FCI_{\text{STO-3G}} | 1048042_{10} \rangle = -0.354$  and  $\langle CI_{1234_{6-31G}} | 68647714816_{10} \rangle = 0.552$  where the base 10 value gives the Slater determinant bitstring when converted to binary. See the raw results and analysis in [36] for further information. For the larger 6-31G problem the size of the underlying search space prevented us from determining whether these other higher-amplitude configurations are truly optimal, leaving open the possibility that even lower-energy solutions remain undiscovered. While more extensive classical resources may further improve the result, moving to larger basis sets (and/or problems) will make the problem classically even more challenging.

In Fig. 6, we present an additional example - linear  $\text{O}_3$  in the triplet state, with each O-O bond set to 2 Å. We compare our search for an improved Fock state solution against results from PySCF using various SCF initialization strategies keeping the MO basis fixed from the optimized PySCF calculation. In nearly all cases (34 out of 36), we identify a lower-energy bitstring, further demonstrating that it is possible to obtain a lower energy single-Fock-state solution in the correct sector. Moreover, these results highlight that there is significant scope for developing new solver heuristics, both classical and quantum. In this example, the cc-pVDZ, cc-pVTZ, and cc-pVQZ basis sets correspond to search spaces of sizes  $\binom{42}{13} \binom{42}{11} \approx 1.09 \times 10^{20}$ ,  $\binom{90}{13} \binom{90}{11} \approx 6.84 \times 10^{28}$  and  $\binom{165}{13} \binom{165}{11} \approx 2.92 \times 10^{35}$ , respectively. The tabulated re-

sults are given in the supporting information S.IV, and the raw results and analysis can be found at [36].

#### IV. UTILITY AND ADVANTAGE FOR GAS-SCF

In quantum computing, advantage refers to problems that a quantum computer can solve but a classical computer cannot. Quantum utility refers to a case where a classical calculation is feasible but a quantum computer can obtain the same result with lower costs in time, space or energy.

The Hartree-Fock SCF problem is equivalent to NP-complete combinatorial optimization problems [19, 20]. In the worst case, it is widely believed that quantum computers cannot solve NP-complete problems in polynomial time. However, exact solutions in the worst case are not the only possibility. Approximate algorithms are evaluated by their *approximation ratio* - the fraction of the exact answer they achieve. Bounds on the approximation ratio achievable by classical algorithms are reasonable targets for quantum advantage. For example, the best approximation ratio achievable by semi-definite programming (SDP) for MAXCUT is 0.878, meaning that SDP will achieve at least this approximation ratio for all instances of MAXCUT [64]. A quantum algorithm that achieved an approximation ratio of  $> 0.878$  for all instances would achieve quantum advantage for MAX-

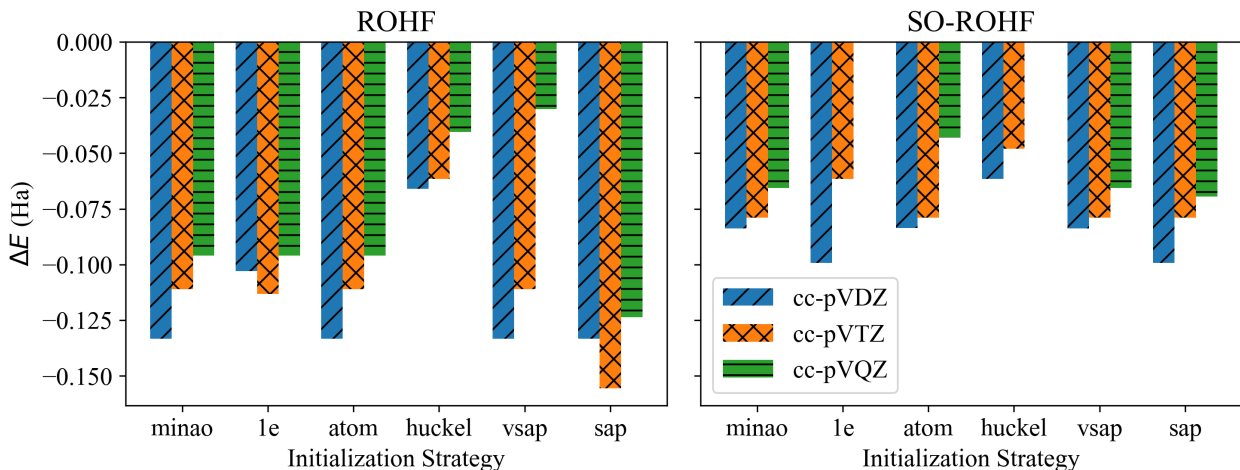


FIG. 6: Comparison of SCF initialization strategies and PySCF solution vs alternate single Fock state solution for triplet  $O_3$ . The y-axis shows the energy error relative to the PySCF (single Fock state) solution (ROHF, left; SO-ROHF, right), computed as  $\Delta E = E_{|x\rangle} - E_{ROHF/SO-ROHF}$ , where  $|x\rangle$  denotes an alternative Fock-state solution.

Lower values of  $\Delta E$  indicate lower energy (better) solutions. The initialization strategies considered include superposition of atomic densities (minao, atom) [58, 59], the core Hamiltonian guess (1e) [60], the parameter-free Hückel guess (huckel) [60], and superposition of atomic potentials (vsap, sap) [60]. Details on each problem can be found in the online repository [36], including the improved Fock state  $|x\rangle$  obtained. The cc-pVDZ, cc-pVTZ, and cc-pVQZ problems correspond to problems with 84, 180, and 330 qubits respectively (excluding ancillary qubits).

## CUT.

The three main algorithms for quantum optimization of combinatorial optimization problems are adiabatic quantum computation (AQC) [25], the quantum approximate optimization algorithm (QAOA) [26], and decoded quantum interferometry (DQI) [27]. There is recent evidence that they may be able to obtain improvements in the approximation ratio for some problems [27, 28]. These results mean that combinatorial optimization is once again a promising target quantum advantage.

In the context of SCF problems, there exist many molecular problems with convergence issues [20, 59, 60, 65–69]. Using classical approaches to approximately solve these hard SCF instances can be used to yield the “best” classical solution. This can be used to seed the initial choice of  $y$  in the GAS-SCF routine. GAS-SCF succeeds if the method outputs a bitstring that surpasses all classical solutions. A key strength of this approach is GAS-SCF marks and boosts the amplitudes of all lower-energy states over the best available classical solution. Such solutions are easy to verify, as they correspond to a single Fock states (single bitstrings). If no better solution is found, one can always fall back on the classical solution. The  $OH^-$  model above illustrates the existence of problem instances where it is possible for GAS-SCF to improve the classical solution. While this small model is well within classical tractability [20], it does indicate that for larger problems that are classically hard to simulate, it may be possible to improve upon classical SCF solutions. The  $O_2$  and  $O_3$  results in this work further

reinforce this point.

SCF calculations are routinely applied to large molecular systems. For example, [70] studies Ubiquitin in the 6-31G\* basis set, for which the Hilbert space dimension is  $2^{2(10273)} \approx 9.168 \times 10^{6184}$ . While [70] demonstrates the feasibility of treating such a system using SCF on conventional computational hardware, the optimality of the resulting classical solutions is not guaranteed, and are unlikely to correspond to the global optimum and are more likely to reflect local minima.

At present, it is not clear whether a classical solver run for an equivalent wall-clock time would offset any advantage of the GAS-SCF routine; addressing this question will require systematic benchmarking studies. Additionally, an alternating hybrid strategy that interleaves quantum and classical SCF iterations may offer further benefits. Ultimately, these possibilities can only be assessed through real execution.

SCF routines are the basis for virtually all post-Hartree-Fock single reference electronic structure methods, such as Møller–Plesset perturbation theory, coupled cluster, and configuration interaction methods. Therefore, any improvement in SCF results in knock-on benefits for the more accurate approaches that build on an SCF solution, by identifying a better molecular orbital basis in which to describe the system.

Quantum algorithms for quantum chemistry, including quantum phase estimation [71, 72], are similarly affected. Here, SCF methods define the MO basis, linearly independent vectors that span the Hilbert space, and there-

fore different choices can alter the support of the ground state. This leads to interrelated consequences: (1) initializing QPE near from a local minimum can be problematic, and (2) the choice of basis influences the support of each eigenstate and thus its overlap with the QPE input state. Improved SCF solutions by GAS-SCF or other quantum optimization techniques offer a means to mitigate both issues.

## V. METHODOLOGY

The PySCF package [73] was used to obtain the molecular integrals needed to construct the Hamiltonian (Equation 2) for linear  $\text{H}_3^-$  and LiH in the STO-3G basis set [74] and  $\text{OH}^-$  in the 6-31G basis set [75] in a (6o, (3e,3e)) active space. The bond lengths studied were 1.0 Å, 1.5 Å and 3.0 Å respectively. A restricted Hartree-Fock (RHF) calculation was performed for each problem. All Hamiltonian operators were then written in the canonical basis, where their coefficients were multiplied by a constant then rounded to integer values in the corresponding QUBO problem. We verified that this method preserved the ground eigenstate. We supply both the original and rounded Hamiltonian data in the online repository [36]. The first solution for the  $\text{OH}^-$  RHF calculation was intentionally chosen as it gives an example of SCF converging onto a local minimum.

These simulations were performed using the statevector method and no actual quantum computers were employed. The python package `symmer` [76] was used to build each chemical Hamiltonian and `Qiskit` [77] was used to simulate the quantum circuits. All the results in this paper can be reproduced by the code provided in the repository [36]. The quantum circuits to generate Dicke states were based on the circuits derived by Bärttschi and Eidenbenz [44], using code modified from [78].

The results for triplet  $\text{O}_2$  at a bond length of 2.55 Å were also obtained using PySCF and `symmer` and can be found on the online repository [36]. An internal stability calculation for this system was performed to ensure that the restricted open-shell Hartree-Fock (ROHF) reference was not a saddle point in both basis sets.

The ROHF and second-order ROHF (Newton method in PySCF) results for linear triplet  $\text{O}_3$  (O–O bond length of 2 Å) were also computed using the cc-pVDZ, cc-pVTZ, and cc-pVQZ basis sets [79] with different initialization strategies and are provided in the online repository [36]. The maximum number of SCF iterations was set to 300 for each calculation. Additionally, up to 10 internal stability checks, each followed by a restarted SCF calculation, were performed to mitigate internal instabilities. A summary of energies and convergence data is provided in the Supporting Information (Section S.IV). The improved solutions were found by performing a brute-force search in the appropriate number symmetry sector, using a 5-minute time limit.

All numerical results in this work were performed on

an Apple M3 MacBook Pro (18 GB RAM).

## VI. CONCLUSION

In this paper, we defined the Grover Adaptive Search Self-Consistent Field (GAS-SCF) routine for SCF chemistry algorithms. We presented complete circuit constructions for two valid implementations: one including a symmetry-flagging step to ensure only solutions within the correct symmetry sector are marked and subsequently amplified, and another which initializes the circuit in a Dicke state and thus restricts us to valid solutions from the beginning.

To investigate the performance of this algorithm, we conducted statevector simulations for several molecular problems. The  $\text{OH}^-$  example, in particular, highlights that the GAS-SCF routine can outperform classical simulation methods: our statevector-based quantum circuit simulation produces a result superior to that of a conventional chemistry package, which converges to a local minimum. Although the classical result could be improved due to the small system size, scaling to larger and more complex problems remains a significant challenge for classical approaches. This scalability limitation underscores the potential for quantum improvements for SCF problems. However, due to the substantial circuit complexity associated with implementing GAS-SCF, large-scale execution of the algorithm remains beyond the capabilities of current quantum hardware.

We then examined some of the criteria required for this algorithm to exhibit quantum advantage, motivating our discussion through a detailed study of triplet  $\text{O}_2$  and  $\text{O}_3$  (linear) - the largest problem considered was 330 qubits. These systems, together with other molecular problems exhibiting SCF convergence challenges, form a promising class of candidate optimization problems. Improvements in approximation ratios for these problems would make them quantum advantage candidates for GAS-SCF, and for other quantum approximation algorithms such as AQC, QAOA and DQI. However, benchmarking against classical heuristics is essential before any claim of quantum advantage can be made.

With respect to quantum speedup, it is important to note that classical SCF solvers rely on heuristic methods, most commonly iterative Fock matrix diagonalization or second-order orbital optimization, rather than exhaustive search. As a result, the quadratic speedup of GAS-SCF (defined relative to brute force) is not comparable to the performance of these classical heuristics. However, it is not an advantage in runtime that could be achieved but an improvement in quality of solution. Solution quality remains an open question for these classical heuristics, as seen here and in approaches such as MaxCut-SCF [20] and GAS-SCF establishes a useful baseline for future quantum improvements of SCF methods.

## ACKNOWLEDGMENTS

A.R. and T.W. are supported by QMatter, Inc. T.M.B. is supported by the Engineering and Physical Sciences Research Council (grant numbers EP/T517793/1,

EP/W524335/1). P.V.C. is grateful for funding from the European Commission for VECMA (800925) and EPSRC for SEAVEA (EP/W007711/1). P.J.L. acknowledge support by the NSF STAQ project (PHY-1818914/232580) and by the NSF NQVL:QSTD:Pilot: Quantum Advantage-Class Trapped Ion system (QACTI) project NSF award number 2410675.

- 
- [1] A. Aspuru-Guzik, A. D. Dutoi, P. J. Love, and M. Head-Gordon, *Science* **309**, 1704 (2005).
- [2] Y. Cao, J. Romero, J. P. Olson, M. Degroote, P. D. Johnson, M. Kieferová, I. D. Kivlichan, T. Menke, B. Peropadre, N. P. Sawaya, *et al.*, *Chemical reviews* **119**, 10856 (2019).
- [3] R. Santagati, A. Aspuru-Guzik, R. Babbush, M. Degroote, L. González, E. Kyoseva, N. Moll, M. Oppel, R. M. Parrish, N. C. Rubin, *et al.*, *Nature Physics* **20**, 549 (2024).
- [4] J. Chen and G. K. Chan, *arXiv preprint arXiv:2508.15765* (2025).
- [5] R. Babbush, N. Wiebe, J. McClean, J. McClain, H. Neven, and G. K.-L. Chan, *Physical Review X* **8**, 011044 (2018).
- [6] R. Babbush, C. Gidney, D. W. Berry, N. Wiebe, J. McClean, A. Paler, A. Fowler, and H. Neven, *Physical Review X* **8**, 041015 (2018).
- [7] I. D. Kivlichan, J. McClean, N. Wiebe, C. Gidney, A. Aspuru-Guzik, G. K.-L. Chan, and R. Babbush, *Physical review letters* **120**, 110501 (2018).
- [8] R. Babbush, D. W. Berry, J. R. McClean, and H. Neven, *npj Quantum Information* **5**, 92 (2019).
- [9] J. Lee, D. W. Berry, C. Gidney, W. J. Huggins, J. R. McClean, N. Wiebe, and R. Babbush, *PRX quantum* **2**, 030305 (2021).
- [10] Y. Su, D. W. Berry, N. Wiebe, N. Rubin, and R. Babbush, *PRX Quantum* **2**, 040332 (2021).
- [11] D. W. Berry, Y. Tong, T. Khattar, A. White, T. I. Kim, G. H. Low, S. Boixo, Z. Ding, L. Lin, S. Lee, *et al.*, *PRX Quantum* **6**, 020327 (2025).
- [12] G. H. Low, R. King, D. W. Berry, Q. Han, A. E. De-Prince III, A. F. White, R. Babbush, R. D. Somma, and N. C. Rubin, *Physical Review X* **15**, 041016 (2025).
- [13] S. Lee, J. Lee, H. Zhai, Y. Tong, A. M. Dalzell, A. Kumar, P. Helms, J. Gray, Z.-H. Cui, W. Liu, *et al.*, *Nature communications* **14**, 1952 (2023).
- [14] H. Zhai, C. Li, X. Zhang, Z. Li, S. Lee, and G. K.-L. Chan, “Classical solution of the femo-cofactor model to chemical accuracy and its implications,” (2026), *arXiv:2601.04621 [physics.chem-ph]*.
- [15] R. Babbush, W. J. Huggins, D. W. Berry, S. F. Ung, A. Zhao, D. R. Reichman, H. Neven, A. D. Baczewski, and J. Lee, *Nature Communications* **14**, 4058 (2023).
- [16] D. R. Hartree, *Mathematical Proceedings of the Cambridge Philosophical Society* **24**, 89–110 (1928).
- [17] A. Szabo and N. S. Ostlund, *Modern Quantum Chemistry: Introduction to Advanced Electronic Structure Theory*, Dover Books on Chemistry (Dover Publications, Mineola, NY, 1996).
- [18] T. Helgaker, P. Jorgensen, and J. Olsen, *Molecular electronic-structure theory* (John Wiley & Sons, 2013).
- [19] J. D. Whitfield and Z. Zimborás, *The Journal of chemical physics* **141** (2014), <https://doi.org/10.1063/1.4903453>.
- [20] A. Ralli, T. Weaving, P. V. Coveney, and P. J. Love, *Journal of Chemical Theory and Computation* **21**, 9511 (2025), pMID: 40985214.
- [21] G. M. J. Barca, D. L. Poole, J. L. G. Vallejo, M. Alkan, C. Bertoni, A. P. Rendell, and M. S. Gordon, in *Proceedings of the International Conference for High Performance Computing, Networking, Storage and Analysis, SC '20* (IEEE Press, 2020).
- [22] A. J. Coleman, in *Reduced-Density-Matrix Mechanics: with applications to many-electron atoms and molecules* (Wiley Online Library, 2007).
- [23] D. A. Mazziotti, *Phys. Rev. Lett.* **106**, 083001 (2011).
- [24] D. A. Mazziotti, *Phys. Rev. A* **102**, 052819 (2020).
- [25] E. Farhi, J. Goldstone, S. Gutmann, J. Lapan, A. Lundgren, and D. Preda, *Science* **292**, 472 (2001).
- [26] E. Farhi, J. Goldstone, and S. Gutmann, “A quantum approximate optimization algorithm,” (2014), *arXiv:1411.4028 [quant-ph]*.
- [27] S. P. Jordan, N. Shutty, M. Wootters, A. Zalcman, A. Schmidhuber, R. King, S. V. Isakov, T. Khattar, and R. Babbush, *Nature* **646**, 831 (2025).
- [28] E. Farhi, S. Gutmann, D. Ranard, and B. Villalonga, *arXiv preprint arXiv:2503.12789* (2025).
- [29] L. K. Grover, in *Proceedings of the Twenty-Eighth Annual ACM Symposium on Theory of Computing, STOC '96* (Association for Computing Machinery, New York, NY, USA, 1996) p. 212–219.
- [30] G. Brassard, P. Høyer, M. Mosca, and A. Tapp, “Quantum amplitude amplification and estimation,” (2002).
- [31] R. Babbush, J. R. McClean, M. Newman, C. Gidney, S. Boixo, and H. Neven, *PRX Quantum* **2**, 010103 (2021).
- [32] T. Hoeffler, T. Häner, and M. Troyer, *Communications of the ACM* **66**, 82 (2023).
- [33] E. Campbell, A. Khurana, and A. Montanaro, *Quantum* **3**, 167 (2019).
- [34] Y. R. Sanders, D. W. Berry, P. C. Costa, L. W. Tessler, N. Wiebe, C. Gidney, H. Neven, and R. Babbush, *PRX Quantum* **1**, 020312 (2020).
- [35] M. Cain, Q. Xu, R. King, L. R. Picard, H. Levine, M. Endres, J. Preskill, H.-Y. Huang, and D. Bluvstein, *arXiv preprint arXiv:2603.28627* (2026).
- [36] A. Ralli and T. Bickley, “Grover Adaptive Search,” <https://github.com/qmatter-labs/GAS> (2025).
- [37] C. Durr and P. Hoyer, “A quantum algorithm for finding the minimum,” (1999), *arXiv:quant-ph/9607014 [quant-ph]*.
- [38] D. Bulger, W. P. Baritomp, and G. R. Wood, *Journal of optimization theory and applications* **116**, 517 (2003).
- [39] D. Thouless, *Nuclear Physics* **21**, 225 (1960).

- [40] A. Gilliam, S. Woerner, and C. Gonsciulea, *Quantum* **5**, 428 (2021).
- [41] W. P. Baritumpa, D. W. Bulger, and G. R. Wood, *SIAM Journal on Optimization* **15**, 1170 (2005).
- [42] T. G. Draper, “Addition on a quantum computer,” (2000), [arXiv:quant-ph/0008033](https://arxiv.org/abs/quant-ph/0008033) [quant-ph].
- [43] F. Orts, G. Ortega, E. Combarro, and E. Garzón, *Journal of Network and Computer Applications* **170**, 102810 (2020).
- [44] A. Bärttschi and S. Eidenbenz, in *Fundamentals of Computation Theory*, edited by L. A. Gąsieniec, J. Jansson, and C. Levcopoulos (Springer International Publishing, Cham, 2019) pp. 126–139.
- [45] A. Bärttschi and S. Eidenbenz, in *2022 IEEE International Conference on Quantum Computing and Engineering (QCE)* (2022) pp. 87–96.
- [46] M. Boyer, G. Brassard, P. Høyer, and A. Tapp, *Fortschritte der Physik: Progress of Physics* **46**, 493 (1998).
- [47] M. A. Nielsen and I. L. Chuang, *Quantum computation and quantum information* (Cambridge university press, 2010).
- [48] H. Ominato, T. Ohyama, and K. Yamaguchi, *IEEE Access* **12**, 74619 (2024).
- [49] G. Brassard, *Science* **275**, 627 (1997).
- [50] L. K. Grover, *Phys. Rev. Lett.* **95**, 150501 (2005).
- [51] T. J. Yoder, G. H. Low, and I. L. Chuang, *Phys. Rev. Lett.* **113**, 210501 (2014).
- [52] D. Cremer, *WIREs Computational Molecular Science* **3**, 482 (2013).
- [53] P. G. Szalay, T. Muller, G. Gidofalvi, H. Lischka, and R. Shepard, *Chemical reviews* **112**, 108 (2012).
- [54] M. Norimoto, R. Mori, and N. Ishikawa, *IEEE Transactions on Communications* **71**, 1926 (2023).
- [55] Q. Sun, *Journal of Computational Chemistry* **36**, 1664 (2015), <https://onlinelibrary.wiley.com/doi/pdf/10.1002/jcc.23981>.
- [56] W. A. Simon, C. M. Gustin, K. Serafin, A. Ralli, G. R. Goldstein, and P. J. Love, *Quantum* **9**, 1953 (2025).
- [57] S. Faro and F. P. Marino, in *Proceedings of the 34th International Symposium on High-Performance Parallel and Distributed Computing*, HPDC '25 (Association for Computing Machinery, New York, NY, USA, 2025).
- [58] J. Almlöf, K. Fægri Jr, and K. Korsell, *Journal of Computational Chemistry* **3**, 385 (1982).
- [59] J. Van Lenthe, R. Zwaans, H. J. Van Dam, and M. Guest, *Journal of computational chemistry* **27**, 926 (2006).
- [60] S. Lehtola, *Journal of chemical theory and computation* **15**, 1593 (2019).
- [61] N. C. Rubin, J. Lee, and R. Babbush, *Journal of Chemical Theory and Computation* **18**, 1480 (2022).
- [62] J. C. Slater, *Phys. Rev.* **34**, 1293 (1929).
- [63] E. U. Condon, *Phys. Rev.* **36**, 1121 (1930).
- [64] M. X. Goemans and D. P. Williamson, in *Proceedings of the twenty-sixth annual ACM symposium on Theory of computing* (1994) pp. 422–431.
- [65] A. D. Daniels and G. E. Scuseria, *Phys. Chem. Chem. Phys.* **2**, 2173 (2000).
- [66] A. C. Vaucher and M. Reiher, *Journal of Chemical Theory and Computation* **13**, 1219 (2017).
- [67] J. Greiner, I.-M. Høyvik, S. Lehtola, and J. J. Eriksen, “A reusable library for second-order orbital optimization using the trust region method,” (2025), [arXiv:2509.13931](https://arxiv.org/abs/2509.13931) [physics.chem-ph].
- [68] N. E. Schultz, Y. Zhao, and D. G. Truhlar, *The Journal of Physical Chemistry A* **109**, 4388 (2005), pMID: 16833770.
- [69] K. N. Kudin and G. E. Scuseria, *ESAIM: Mathematical Modelling and Numerical Analysis* **41**, 281–296 (2007).
- [70] E. Palethorpe, R. Stocks, and G. M. J. Barca, *Journal of Chemical Theory and Computation* **20**, 10424 (2024), pMID: 39586097.
- [71] A. Y. Kitaev, “Quantum measurements and the abelian stabilizer problem,” (1995), [arXiv:quant-ph/9511026](https://arxiv.org/abs/quant-ph/9511026) [quant-ph].
- [72] R. Babbush, P. J. Love, and A. Aspuru-Guzik, *Scientific reports* **4**, 6603 (2014).
- [73] Q. Sun, X. Zhang, S. Banerjee, P. Bao, M. Barbry, N. S. Blunt, N. A. Bogdanov, G. H. Booth, J. Chen, Z.-H. Cui, *et al.*, *The Journal of chemical physics* **153** (2020), <https://doi.org/10.1063/5.0006074>.
- [74] W. J. Hehre, R. F. Stewart, and J. A. Pople, *The Journal of Chemical Physics* **51**, 2657 (1969).
- [75] W. J. Hehre, R. Ditchfield, and J. A. Pople, *The Journal of Chemical Physics* **56**, 2257 (1972).
- [76] A. Ralli and T. J. Weaving, “symmer,” <https://github.com/qmatter-labs/symmer> (2025).
- [77] A. Javadi-Abhari, M. Treinish, K. Krsulich, C. J. Wood, J. Lishman, J. Gacon, S. Martiel, P. D. Nation, L. S. Bishop, A. W. Cross, B. R. Johnson, and J. M. Gambetta, “Quantum computing with Qiskit,” (2024), [arXiv:2405.08810](https://arxiv.org/abs/2405.08810) [quant-ph].
- [78] A. Juan, “Dicke states preparation,” [https://github.com/andre-juan/dicke\\_states\\_preparation/](https://github.com/andre-juan/dicke_states_preparation/) (2025).
- [79] T. H. Dunning Jr, *The Journal of chemical physics* **90**, 1007 (1989).
- [80] C. Gidney, *Quantum* **2**, 74 (2018).

## SUPPORTING INFORMATION

This document provides the Supporting Information for the main paper. It includes background on quantum arithmetic (Sec. [S.I](#)) and two's complement representation (Sec. [S.II](#)), as well as a complete description of the quantum circuit components required to implement GAS-SCF introduced in the main text (Sec. [S.III](#)). Sec. [S.IV](#) provides the raw results for the  $O_3$  result, including convergence information. Finally, Sec. [S.V](#) provides an alternate compilation for GAS-SCF.

### S.I. FOURIER BASIS AND ADDITION

In this section, we summarize the work of Draper [\[42\]](#), who demonstrated how to perform arithmetic operations on a quantum computer using the Fourier basis.

The quantum Fourier transform (QFT) can be written as:

$$\begin{aligned}
 |a\rangle &= |a_1 a_2 \dots a_\omega\rangle \\
 &\xrightarrow[\text{QFT}]{\text{QFT}^\dagger} \\
 \frac{1}{\sqrt{2^\omega}} \sum_{k=0}^{2^\omega-1} e^{2\pi i a k / 2^\omega} |k\rangle &= \frac{1}{\sqrt{2^\omega}} \sum_{k=0}^{2^\omega-1} e^{2\pi i (\sum_{l=1}^{\omega} k_l / 2^l) a} |k_1 k_2 \dots k_\omega\rangle \\
 &= \frac{1}{\sqrt{2^\omega}} \sum_{k=0}^{2^\omega-1} \prod_{l=1}^{\omega} e^{2\pi i a k_l / 2^l} |k_1 k_2 \dots k_\omega\rangle \\
 &= \frac{1}{\sqrt{2^\omega}} \bigotimes_{l=1}^{\omega} \left( |0\rangle + e^{2\pi i a / 2^l} |1\rangle \right) \\
 &= \left( |0\rangle + e^{2\pi i a / 2^1} |1\rangle \right) \otimes \left( |0\rangle + e^{2\pi i a / 2^2} |1\rangle \right) \otimes \dots \otimes \left( |0\rangle + e^{2\pi i a / 2^\omega} |1\rangle \right) \\
 &= |\phi_1(a)\rangle \otimes |\phi_2(a)\rangle \otimes \dots \otimes |\phi_\omega(a)\rangle,
 \end{aligned} \tag{S.1}$$

where:

$$|\phi_j(a)\rangle = \frac{1}{\sqrt{2}} \left( |0\rangle + e^{2\pi i a / 2^j} |1\rangle \right). \tag{S.2}$$

We observe that in the final two lines of Equation [S.1](#), the output is represented as a tensor product of single-qubit states, which corresponds to a product state <sup>1</sup>. Each single-qubit state can therefore be prepared using a single quantum phase gate  $P(\theta)$ :

$$P(\theta) = \begin{bmatrix} 1 & 0 \\ 0 & e^{i\theta} \end{bmatrix}, \tag{S.3}$$

applied on qubit  $j \in [1, \omega]$ , in the  $|+\rangle = H|0\rangle = \frac{1}{\sqrt{2}}(|0\rangle + |1\rangle)$  state. The angle of rotation given  $a$  is obtained via:

$$\theta = \frac{2\pi a}{2^j} = \frac{\pi a}{2^{j-1}}. \tag{S.4}$$

The gate is equivalent to a  $R_z$  gate up to a phase factor:  $P(\theta) = e^{i\theta/2} R_z(\theta)$ .

Overall, given a computational basis state (the binary representation of an integer), we can express this state directly in the Fourier basis by applying single-qubit Hadamard and phase gates to each qubit. Next, we will see how this idea enables addition in the Fourier basis.

---

<sup>1</sup> This holds only for input states that are single computational basis states.

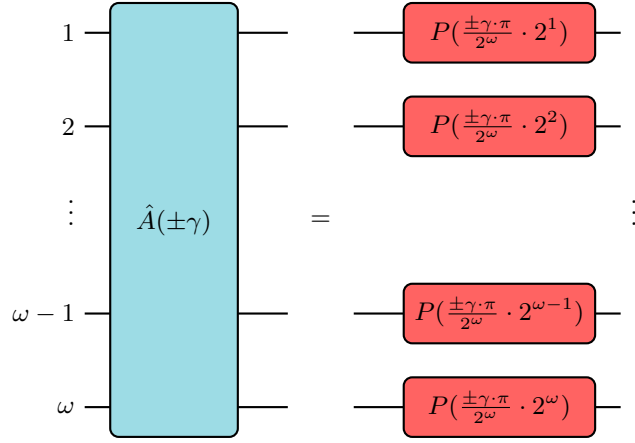


FIG. S.1: Quantum addition circuit operating on  $\omega$ -qubits in the Fourier basis, assuming each qubit is unentangled and its Bloch vector lies in the XY-plane. The single qubit phase gate  $P$  is defined in Equation S.3.

The quantum “adder” works due to the fact that rotations along the same direction (about the same axis) in  $\text{SO}(3)$  combine by simple addition of their angles. Therefore:

$$\begin{aligned}
 \hat{A}(x)\hat{A}(m)H^{\otimes m}|0\rangle &= \hat{A}(x_1, x_2, \dots, x_\omega)\hat{A}(m_1, m_2, \dots, m_\omega)|+\rangle \\
 &= \hat{A}(m_1 + x_1, m_2 + x_2, \dots, m_\omega + x_\omega)|+\rangle \\
 &= (|0\rangle + e^{2\pi i(m+x)/2^1}|1\rangle) \otimes (|0\rangle + e^{2\pi i(m+x)/2^2}|1\rangle) \otimes \dots \otimes (|0\rangle + e^{2\pi i(m+x)/2^l}|1\rangle) \quad (\text{S.5}) \\
 &\xrightarrow{QFT^\dagger} |(m+x) \bmod 2^\omega\rangle.
 \end{aligned}$$

Geometrically, Hadamard gates first map each qubit onto the XY-plane. Phase gates are then used to rotate the Bloch vector of each qubit around the Z-axis. Each rotation represent the addition of a different integer. The inverse QFT transform is then used to interfere these carefully constructed phases such that they produce the desired binary output. Figure S.1 shows the quantum circuit required to implement  $\hat{A}$ .

The next Section shows how binary can be used to represent signed integers.

## S.II. TWO’S COMPLIMENT

Two’s complement is a method of representing signed integers (positive and negative). In this system, the most significant bit (the left-most bit) determines the sign: 0 for non-negative numbers and 1 for negative numbers. Figure S.2 illustrates this using a 4-bit clock. On the signed clock (Figure S.2b), the value at the top is zero. Moving clockwise increases the value in positive steps, while moving counter-clockwise decreases it in negative steps. In contrast, the unsigned clock (Figure S.2a) contains only non-negative values, encoded in standard binary. Both systems span the same total number of representable states  $2^n$ ; for  $n = 4$  this is 16. The signed clock has the integer range  $[-2^{n-1}, 2^{n-1}) \cap \mathbb{Z} \equiv \{-8, -7, -6, -5, -4, -3, -2, -1, 0, 1, 2, 3, 4, 5, 6, 7\}$  and the unsigned clock covers  $[0, 2^n) \cap \mathbb{Z} \equiv \{0, 1, 2, 3, 4, 5, 6, 7, 8, 9, 10, 11, 12, 13, 14, 15\}$ .

There is an important structural pattern visible in the signed clock (Figure S.2b). If we ignore the most significant (leftmost) bit, the sequences  $0 \mapsto 7$  and  $-8 \mapsto -1$  each use the standard binary encodings 000 through 111. The positive range follows the standard counting order, and the negative values follow the reverse order. If we could “flip” the negative region so that the magnitude of the number is represented in standard binary then we would have the entire number line would be represented contiguously in binary. Two’s complement achieves exactly this: it reinterprets the bit patterns so that the negative numbers wrap around and appear after the positive ones in standard binary order. The same structure arises for an arbitrary  $n$ -bit binary clock, not just the 4-bit example.

To determine the value of a number encoded in two’s complement, we follow the procedure summarized in Algorithm in Figure S.3. If the most significant (left-most) bit is 1, the encoded number is negative. Its magnitude can be obtained by inverting all bits, adding one, and then converting the resulting bitstring from binary to its base-10 value; the final result is the negation of this value. If the most significant bit is 0, the bitstring is interpreted using the standard

binary-to-decimal conversion. This process of invert and add one is precisely the “flip” referred to in the previous paragraph, which aligns the negative portion of the number line with the standard binary ordering for representing the magnitude of the negative number.

Take the binary number 1110 as an example. Since the leftmost bit is 1, it represents a negative number in two’s complement form. First, invert all the bits:  $1110 \mapsto 0001$ . Then, add 1 to the result:  $0001_2 + 1_{10} = 1_{10} + 1_{10} = 2$ . Finally, apply the negative sign:  $-2$ . So, in decimal,  $1110_2 = -2_{10}$ . We could also work this out in the integer representation. Here  $1110_2$  is  $14_{10}$  in standard binary, but in two’s complement we get  $-(2^4 - 14) = -(16 - 14) = -2$ .

In conventional modular arithmetic, subtraction (moving anti-clockwise) can be represented by addition (moving clockwise). In further detail, for mod  $w$ , we note that subtracting  $x$  is the same as adding  $(w - x) \bmod w$ , where it is assumed  $0 \leq x \leq w$ . As an example, take a look at Figure S.4a. If we wanted to subtract 4 from 2:  $(2 - 4) \bmod 2^4 = -2 \bmod 16 = 14$ . This is the same thing as adding (moving clockwise):  $(2^4 - 4) \bmod 2^4 = (16 - 4) \bmod 16 = 12 \bmod 16 = 12$ . Moving the green arrow at 2 clockwise twelve units is the same thing as subtracting, moving anticlockwise, four units.

In Two’s Complement representation, the same thing is true. The number line has just been shifted from  $[0, 2^n)$  to  $[-2^{n-1}, 2^{n-1})$ . The movement of the clock acts in the same way. As an example, in Figure S.4b if we wanted to subtract four from two we see that in the same way we either move clockwise twelve units (addition) or moving anticlockwise (subtraction) four units. The only difference is now the encoding represents  $-2$  rather than 14 in standard binary.

Two’s complement preserves the usual behaviour of addition and subtraction on the integer number line; deviations arise only when an operation exceeds the representable range and overflow occurs. For instance, in the 4-bit system, subtracting 12 from two would ordinarily yield  $-10$ ; however, the result wraps to 6 because  $-10$  cannot be represented with only four bits in this encoding.

In two’s-complement encoding with  $\omega$ -bits, any integer in the range  $-2^{\omega-1} \leq a < 2^{\omega-1}$ , including negative values, can also be represented using the phases defined in Equation S.4.

For Grover Adaptive Search the defining characteristic of this encoding is that the leftmost qubit serves as an indicator of whether the corresponding base-10 value is negative. In the GAS quantum circuit, this qubit is specifically employed to control the marking oracle, thereby enabling the phase adjustment (marking) of lower-energy states for Grover’s search. As illustrated in Figure 2 and Figure 3 in the main text, the *sign* qubit is positioned directly beneath the register of  $m$  qubits.

In the next Section we discuss each component of the GAS quantum circuit for GAS-SCF.

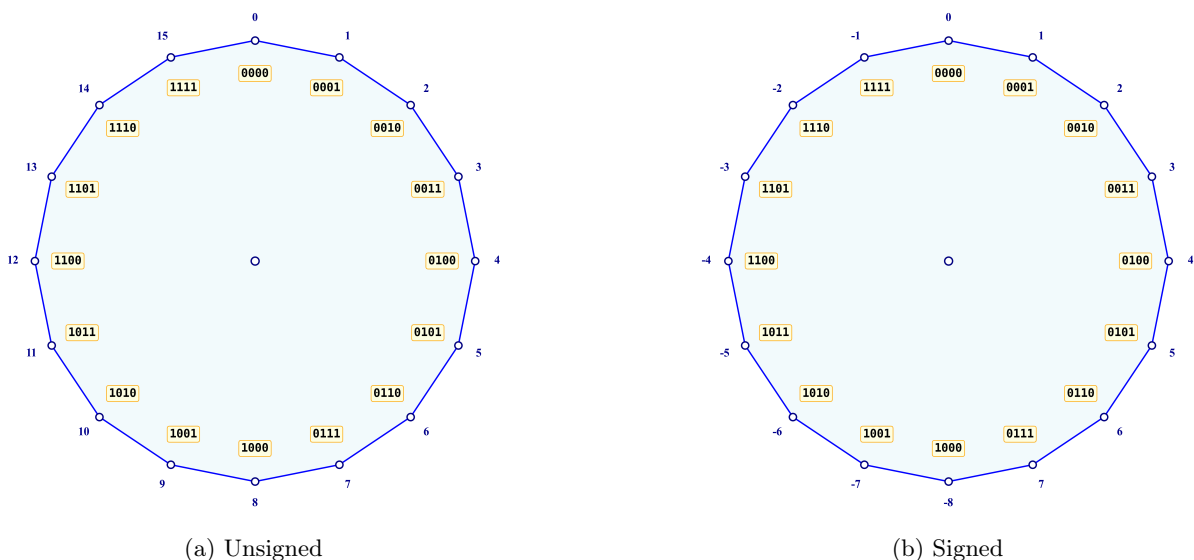


FIG. S.2: Clock-face illustration of four-bit signed and unsigned binary integer representations.

---

```

1: Input:  $[b_1, b_2, \dots, b_\tau]$  where  $b_i \in \{0, 1\}$ 
2:
3: if  $b_1 == 1$  then
4:    $out \leftarrow -(1 + \sum_{j=1}^{\tau} \lfloor \frac{b_{j+1}}{2} \cdot 2^{\tau-j} \rfloor)$ 
5: else
6:    $out \leftarrow \sum_{j=1}^{\tau} b_j \cdot 2^{\tau-j}$ 
7: end if
8:
9: Return:  $out \in [-2^{\tau-1}, 2^{\tau-1}]$ 

```

---

FIG. S.3: Algorithm to convert a two's complement  $\tau$ -bit binary number to signed decimal.

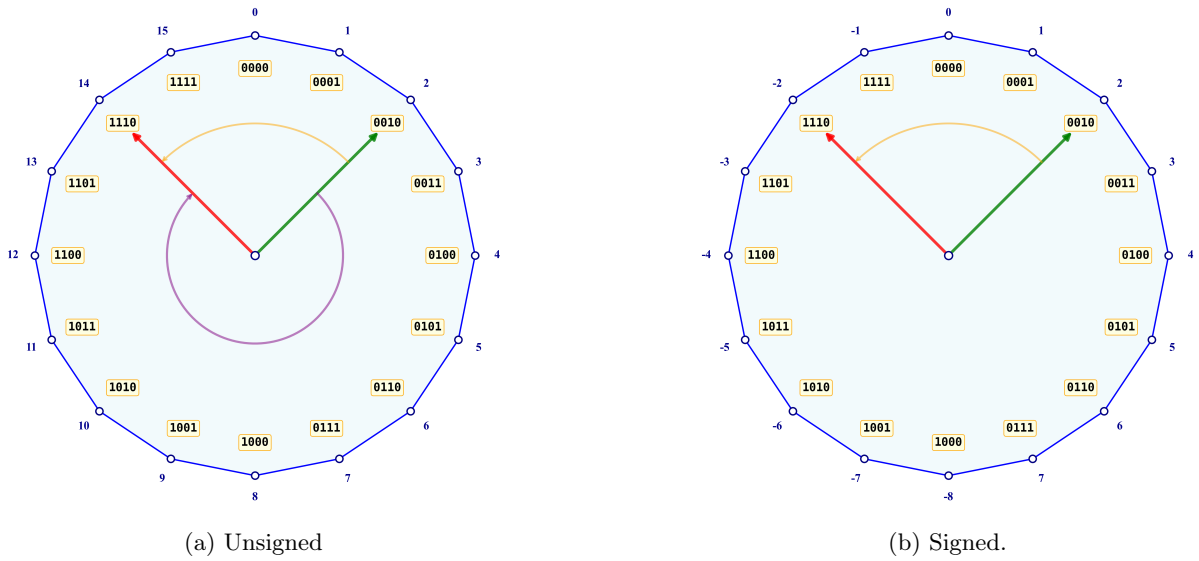


FIG. S.4: Clock-face illustration demonstrating how addition and subtraction coincide in modular arithmetic. In this case, adding 12 produces the same result as subtracting 4 (in mod 16).

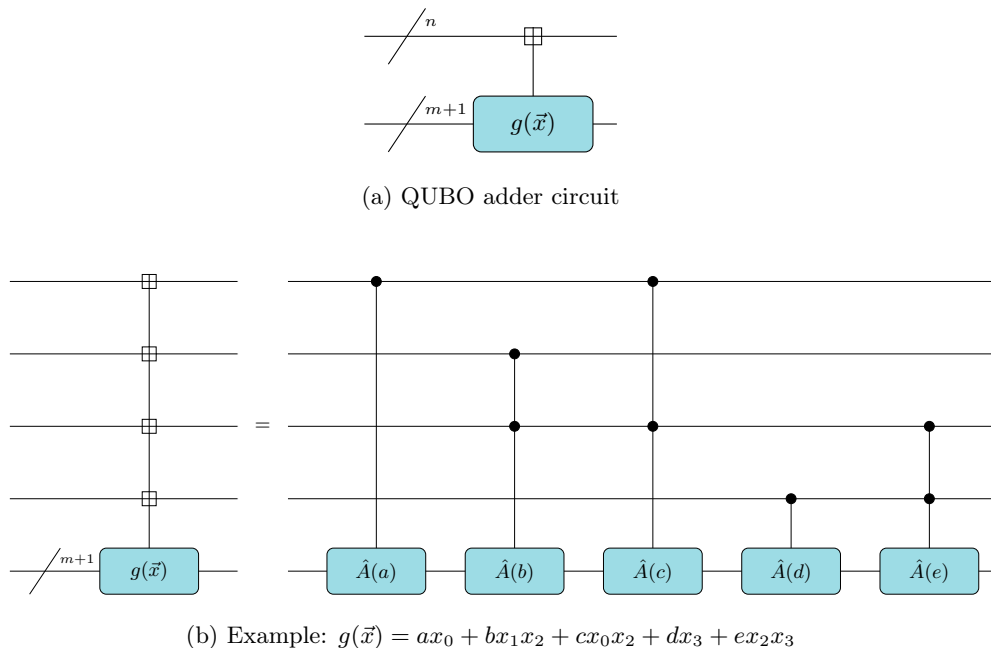


FIG. S.5: Quantum circuits to implement addition in a polynomial Boolean function. (a) Shows the generic circuit and (b) Provides a simple example where each coefficient is a positive/negative integer:  $\{a, b, c, d, e\} \in \mathbb{Z}$ . We assume here the  $m + 1$  qubits is enough to store the maximum value of the Boolean function  $|g(\vec{x})|$ . Each  $\hat{A}$  gate is defined in Figure S.1. Note that each qubit in the  $m + 1$  register is assumed to have been rotated into the XY-plane. This circuit produces the sum in the Fourier basis, which can be converted back to the computational (decimal) basis using the inverse QFT.

### S.III. GAS-SCF QUANTUM CIRCUIT COMPONENTS

In this section we detail all the non-standard circuit components required to implement GAS-SCF.

Gilliam, Woerner, and Gonciulea [40] showed how to implement a pseudo-Boolean function via a quantum circuit. We summarize their approach in Figure S.5. However, for SCF simulations we also require solutions to be in the correct symmetry sector. We can write the number operator as a Boolean function composed of linear terms:

$$\hat{N}_\alpha(\vec{x}) = \sum_{i \in \mathcal{A}} x_i, \quad (\text{S.6a})$$

$$\hat{N}_\beta(\vec{x}) = \sum_{i \in \mathcal{B}} x_i, \quad (\text{S.6b})$$

where  $\mathcal{A}$  and  $\mathcal{B}$  contain the spin indices for the spin-up and spin-down electrons respectively. Both these functions can be implemented according to the circuits in Figure S.5. Here each polynomial term is linear and thus at most each term will require a single control.

To ensure that the correct number of particles is ensured, we need to flag all bitstrings that have the correct Hamming weight. Figure S.6 details the general quantum circuit required for  $\gamma$  electrons.

Note that the control sequence is used to find all states with a particular occupation number (Hamming weight). For example, on the system register  $|0111110\rangle$ ,  $|1011101\rangle$  and  $|1101011\rangle$  all have  $N(x) = 5$  electrons. Running  $N(x)$  (Figure S.6) applied to these input states, results in  $|101\rangle$  being stored in the  $N_{\gamma(x)}$  register (post  $QFT^\dagger$ ). We see that Figure S.6b would therefore flag these states. In other words, this circuit should not be mistaken for selecting the state  $|101\rangle$  in the system register.

Next, a quantum circuit is required for marking quantum states that are  $f(\vec{x}) - y < 0$  in the  $m + 1$  qubit register (and potentially states with the correct symmetries). In GAS, single ancilla qubits in the  $|1\rangle$  state are used to herald when states obey the required constraints. To mark these states therefore only requires controlling off these ancilla

qubits. Figure S.7 shows how this unitary can be compiled as a quantum circuit. These templates stem from the following circuit identity:

$$\begin{aligned}
CNOT(0,1) \cdot [I_0 \otimes R_z(-2\pi)_1] \cdot CNOT(0,1) &= CNOT(0,1) \cdot [I_0 \otimes -I_1] \cdot CNOT(0,1) \\
&= \left( -|0\rangle\langle 0| \otimes I - |1\rangle\langle 1| \otimes X \right) \cdot \left( |0\rangle\langle 0| \otimes I + |1\rangle\langle 1| \otimes X \right) \\
&= -|0\rangle\langle 0| \otimes I - |1\rangle\langle 1| \otimes I \\
&= \frac{1}{2} \left( -(I+Z) \otimes I - (I-Z) \otimes I \right) \\
&= \frac{1}{2} \left( -II - ZI - II + ZI \right) \\
&= \frac{2(-II)}{2} = -II.
\end{aligned} \tag{S.7}$$

We could have also leveraged the fact that the identity matrix commutes with all operators to move the  $CNOT$  gates and cancel them out. The cascade of  $CNOT$  gates enforces a global  $-(I^{\otimes \omega})$  operation across all qubits. In contrast, if the qubits were not fully entangled, applying a single  $R_z(-2\pi)$  rotation would introduce a relative phase rather than a uniform global phase.

Finally, Figure S.8 shows how the reflection step can be compiled efficiently as a quantum circuit.

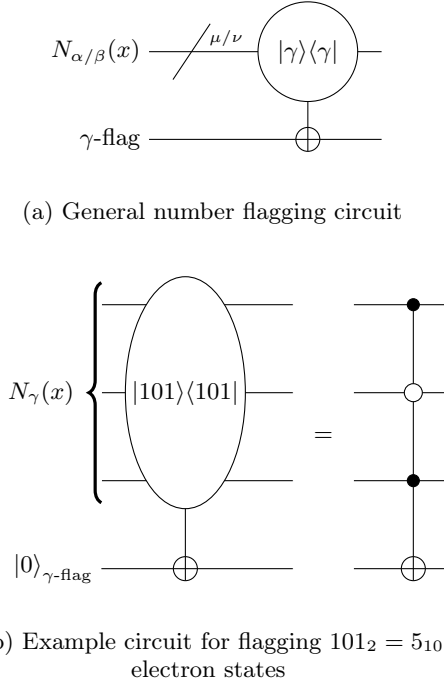


FIG. S.6: Quantum circuits to flag equality constraint needed for ensuring correct number of electrons. Note it is assumed that the  $N_{\gamma \in \{\alpha, \beta\}}(x)$  register has stored the number of electrons according to Equation S.6 implemented by a circuit in Figure S.5 followed by an inverse QFT so that the occupation numbers are represented in the computational basis rather than Fourier basis. We show the full structure in Figure 2. (a) Shows the generic circuit for  $\gamma$  electrons. (b) Provides a simple example for  $\gamma = 5_{10} = 101_2$ .

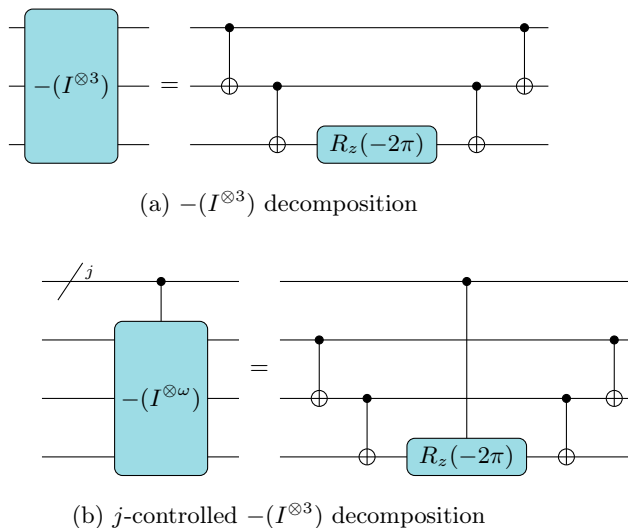


FIG. S.7: Quantum circuits to implement  $-I$  operation on  $\omega$ -qubits. (a) Quantum circuit template to implement  $-(I^{\otimes \omega})$  by recursively applying Equation S.7. (b) Efficient implementation of the multi-control  $-(I^{\otimes 3})$  operator.

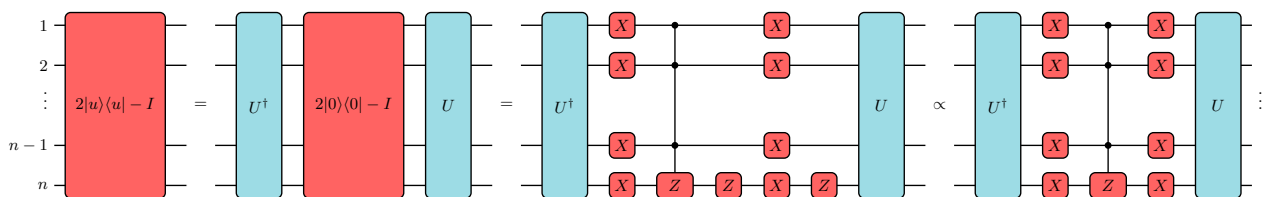


FIG. S.8: Quantum circuit to implement reflection around  $|u\rangle = U|0\rangle$ . In the context of this work, the unitary  $U$  will either prepare:  $U|0\rangle = |s\rangle = H^{\otimes n}|0\rangle$  or  $U|0\rangle = |d\rangle$  (Dicke state). Note final right hand circuit is the same up to a global phase of  $-1$ . This circuit implements  $(2|u\rangle\langle u| - I)|\psi\rangle = U(2|0\rangle\langle 0| - I)U^\dagger|\psi\rangle$  for an arbitrary input state  $|\psi\rangle$ .

### S.IV. LINEAR (TRIPLET) O<sub>3</sub> RESULTS

Tables IIa and IIIa present the raw results corresponding to Fig.6. Tables IIb and IIIb provide the associated convergence data. All data is also available online at [36].

(a) $\Delta E$ results				(b) Convergence results			
	cc-pVDZ	cc-pVTZ	cc-pVQZ		cc-pVDZ	cc-pVTZ	cc-pVQZ
minao	-0.133417	-0.111145	-0.096022	minao	(True, False)	(True, False)	(True, False)
1e	-0.102889	-0.113272	-0.096023	1e	(True, True)	(True, False)	(True, False)
atom	-0.133414	-0.111131	-0.096023	atom	(True, False)	(True, False)	(True, False)
huckel	-0.066024	-0.061446	-0.040510	huckel	(True, True)	(True, True)	(True, True)
vsap	-0.133417	-0.111145	-0.030269	vsap	(True, False)	(True, False)	(True, False)
sap	-0.133414	-0.155568	-0.123688	sap	(True, False)	(True, True)	(True, True)

TABLE II: Left: Raw energy (Ha) results for the improved O<sub>3</sub> solution compared to the PySCF ROHF solution (see Fig. 6, left). Right: Convergence data for the ROHF PySCF solution of O<sub>3</sub>, where each entry is a Boolean tuple (SCF converged, SCF internally stable).

(a) $\Delta E$ results				(b) Convergence results			
	cc-pVDZ	cc-pVTZ	cc-pVQZ		cc-pVDZ	cc-pVTZ	cc-pVQZ
minao	-0.083761	-0.078899	-0.065517	minao	(True, True)	(True, True)	(True, True)
1e	-0.099283	-0.061475	0.000000	1e	(True, True)	(True, True)	(True, True)
atom	-0.083609	-0.078899	-0.042935	atom	(True, True)	(True, True)	(True, True)
huckel	-0.061620	-0.048055	0.000000	huckel	(True, True)	(True, True)	(True, True)
vsap	-0.083761	-0.078899	-0.065517	vsap	(True, True)	(True, True)	(True, True)
sap	-0.099283	-0.078898	-0.069503	sap	(True, True)	(True, True)	(True, True)

TABLE III: Left: Raw energy (Ha) results for the improved O<sub>3</sub> solution compared to the PySCF SO-ROHF (newton) solution (see Fig. 6, right). Right: Convergence data for the SO-ROHF PySCF solution of O<sub>3</sub>, where each entry is a Boolean tuple (SCF converged, SCF internally stable).

### S.V. FAULT TOLERANT COMPILATION

Simon *et al.* [56, Appendix D] describe how to perform quantum arithmetic for known classical integer values. These results can be applied directly to obtain the  $T$ -gate cost for GAS-SCF (note other adder constructions are also possible). Figures S.9 and S.10 summarize the adder circuits required. The implementation of the singly controlled adder circuit requires  $4(m-1)$   $T$  gates and  $(m-1)$  clean ancilla qubits [56]. Each doubly controlled adder circuit (Fig. S.10) incurs an additional cost of 4  $T$  gates and one extra ancilla, bringing the total to  $4m$   $T$  gates with  $m$  clean ancilla [56, 80]. Importantly, this approach maintains the cost function values in two's complement representation (without using the Fourier basis), and therefore does not require an inverse quantum Fourier transform. Table IV provides a summary of the overall gate costs for a single iteration. In this realization  $\mathcal{O}(m)$  extra ancilla qubits are required for the adder circuits controlled from the QUBO register onto the  $m+1$  register and  $\mathcal{O}(n)$  additional ancilla qubits for the adder circuits controlled from the QUBO register storing the number of electrons in the  $\nu$  and  $\mu$  registers. This  $\mathcal{O}(n)$  extra ancilla is not required for the Dicke realization, as the search space is already in the correct number sector.

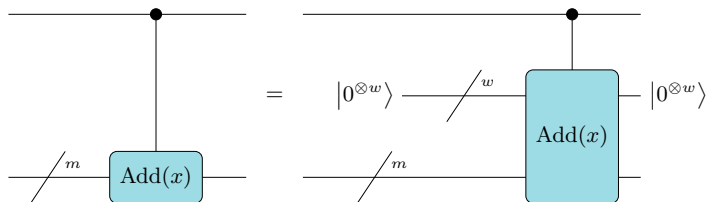


FIG. S.9: General singly controlled adder circuit. The number of clean ancilla required is  $w = m - 1$ . See [56, Appendix D] for how to compile the adder circuit fully.

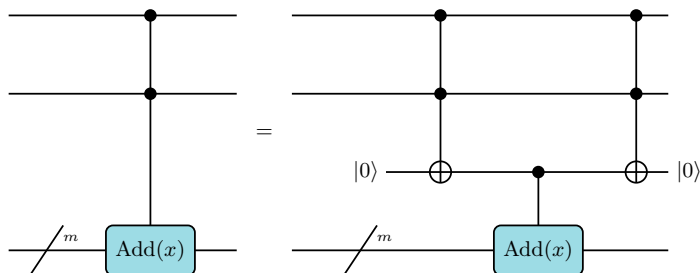


FIG. S.10: General doubly controlled adder circuit. This construction uses a single additional ancilla qubit to store the parity of the control qubits, after which a singly controlled adder (Fig. S.9) is applied. Gidney [80] demonstrates that this can be implemented efficiently using four  $T$  gates together with a conditioned controlled- $Z$  operation.

	Gate Type	Gate Count	Asymptotic Gate count	Asymptotic T count	Note
(1)	Singly-controlled Adder	At most $2n$	$\mathcal{O}(n)$	$\mathcal{O}(nm)$	$f(\vec{x})$ linear terms
	Doubly-controlled Adder	At most $2\binom{n}{2}$	$\mathcal{O}(n^2)$	$\mathcal{O}(n^2m)$	$f(\vec{x})$ quadratic terms
	$(n-1)$ -controlled $Z$	1	$\mathcal{O}(1)$	$\mathcal{O}(n)$	For $2 0^{\otimes n}\rangle\langle 0^{\otimes n}  - I^{\otimes n}$ reflection
	$X$	$2n$	$\mathcal{O}(n)$	0	For $2 0^{\otimes n}\rangle\langle 0^{\otimes n}  - I^{\otimes n}$ reflection
	$CNOT$	$2(n-1)$	$\mathcal{O}(n)$	0	For marking operation
(2)	Singly-controlled Adder	$2n$	$\mathcal{O}(n)$	$\mathcal{O}(nm)$	$\tilde{N}_{\alpha/\beta}(x)$ linear terms
	$\mu$ -controlled $X$	2	$\mathcal{O}(1)$	$\mathcal{O}(n)$	To mark correct Hamming weight states ( $\alpha$ electrons)
	$\nu$ -controlled $X$	2	$\mathcal{O}(1)$	$\mathcal{O}(n)$	To mark correct Hamming weight states ( $\beta$ electrons)
	Toffoli	2	$\mathcal{O}(1)$	$\mathcal{O}(1)$	Check for correct number of $\alpha$ & $\beta$ electrons
(3)	$H$	$2n$	$\mathcal{O}(n)$	0	To reflect around $ s\rangle$ on $n$ -qubits
	Doubly-controlled $R_Z(-2\pi)$	1	$\mathcal{O}(1)$	$\mathcal{O}(1)$	For marking operation
(4)	Dicke state construction. See <i>e.g.</i> [44, 45]	$2(w(n/2, n_\alpha) + w(n/2, n_\beta))^a$	$\mathcal{O}(kn) \leq \mathcal{O}(n^2)^b$	[44]	To reflect around $ d\rangle$ on $n$ -qubits
	Singly-controlled $R_Z(-2\pi)$	1	$\mathcal{O}(1)$	0	For marking operation

<sup>a</sup>  $w(n, k)$  used as a placeholder for quantum circuit cost to generate  $\binom{n}{k}$  Dicke state.

<sup>b</sup> Scaling for the Dicke circuit implementation we used is at worst quadratic when  $k = \mathcal{O}(n)$  [44]; other approaches may differ.

TABLE IV: Gate requirements for one repetition of GAS-SCF that is repeated  $L$  times. Adder circuits for this implementation are given in Figures S.9 and S.10. The table is broken into four sections as follows: (1), gates required for both  $|s\rangle$  and  $|d\rangle$  algorithms; (2), extra gates required to enforce occupation numbers (for  $|s\rangle$  version only); (3), extra gates required for reflection (for  $|s\rangle$  version only); (4), extra gates required for reflection (for  $|d\rangle$  version only). Here  $\alpha$  and  $\beta$  denote the number of spin-up and spin-down electrons respectively. Note no  $QFT^\dagger$  is required. In this realization  $\mathcal{O}(m+n)$  extra ancilla qubits are required for the adder circuits for  $|s\rangle$  and  $\mathcal{O}(m)$  for  $|d\rangle$ .